Improving the Classification of High Relief RADARSAT Imagery Through the Fusion of Ascending and Descending Look Angle Images.

By

Richard John Sykes
B.Sc., University of Victoria, 1980

A Thesis Submitted in Partial Fulfillment of the Requirements
for the Degree of

MASTER OF SCIENCE

in the Department of Geography

We accept this thesis as conforming to
the required standard

[redacted]

Dr. Olaf Niemann, Supervisor (Department of Geography)

[redacted]

Dr. Stanton Tuller, Member (Department of Geography)

[redacted]

Dr. Ian Barrodale, Outside Member (Adjunct, Department of Computer Science)

[redacted]

Dr. Gerard McLean, External Examiner (Department of Mechanical Engineering)

Supervisor: Dr. K.O. Niemann

ABSTRACT

The interpretation of Synthetic Aperture RADAR (SAR) imagery is impacted by viewing direction and the visual effects of foreshortening, shadowing, and layover. In areas of high relief, these effects of topography are amplified to the extent that classifications of opposite side imagery of the same area can vary significantly. Traditionally, to compensate for these distortions, digital elevation models (DEMs) have been employed to either ortho correct the imagery, or to create synthetic SAR images. This paper explores a data fusion approach to SAR interpretation. Opposite side (ascending/descending) RADARSAT imagery are fused to create a single image combining the interpretable features contained in both input images. Each member of the image pair is geocorrected using British Columbia Terrain Resource Information Management (TRIM) planimetric data, fused, and the resultant images then compared to the originals using TRIM DEM data.

Examiners:

[redacted]

Dr. K.O. Niemann, Supervisor (Department of Geography)

[redacted]

Dr. Stanton Fuller, Member (Department of Geography)

[redacted]

Dr. Ian Barrodale, Outside Member (Adjunct, Department of Computer Science)

[redacted]

Dr. Gerard McLean, External Examiner (Department of Mechanical Engineering)

Table of Contents

Chapter 6: Conclusions

LIST OF FIGURES

LIST OF TABLES

Acknowledgments

First of all I would like to thank my supervisor, Olaf Niemann, for accepting me as a graduate student, supporting a number of thesis projects (including this, the final one) and being in my corner when the outcome was in doubt. I would also like to thank my committee; Stan Tuller for his careful reading of my drafts and Ian Barrodale for saying the thesis might be of some use. Thanks also, to the Department of Geography, University of Victoria for providing a great job and the opportunity and encouragement to pursue a higher degree. Finally, I would like to thank the external examiner Ged McLean for endeavoring to make sure the degree was worth having.

Chapter 1

Introduction

1.0 Introduction

There are two possible avenues of research with regard to a sensor product. First, find the kinds of applications that are particularly suited to the product, and second, find processes that can be applied to the product to make it suitable for an application. With regards to active microwave remote sensing, some applications utilize the ability to 'see' through cloud cover both day and night, or the ability to penetrate some ground covers. Other applications take advantage of the texture, tone, and edge determinations possible through microwave remote sensing, or the possibility of creating accurate digital terrain models. An example of processes applied to a product to make it suitable for an application would be the geocorrection of an image using ancillary information such as ground control points or vector data. The utility of an image product can also be enhanced by combining it with another image product.

The fact that active microwave remote sensing can provide ground images in all light and weather conditions is only notable if those images contain information of some value. Identified applications that find value in microwave imagery include agriculture, forestry, urban classification, archaeology, coastal processes, oceanography, hydrology, geology, and geomorphology (Brown *et al.*, 1996). Applications in agriculture are based on Radar's sensitivity to moisture and ability to differentiate between variations in texture (see chapter two for details). Sensitivity to moisture is important in determining irrigation needs while texture analysis is useful in determining soil types or maturity of crop covers. These same attributes are applicable to the study of forests through active microwave sensing. Wilson (1996) demonstrated the value of microwave imagery in estimating coniferous forest structure. Using texture and tone

valuations in airborne Synthetic Aperture RADAR (SAR) imagery Wilson produced classifications differentiating pine and spruce stands of different height and closure types. A similar study by Ahern *et al.* (1996) also used tone and texture to classify forest type and structure, differentiating between hardwoods and softwoods on a seasonal basis.

While tone and texture are principally used to classify ground covers, the prominence of edges in microwave imagery is of value to other applications. The ability to detect linear features is useful in urban environments, where the linear finger print of man-made features is readily apparent (Heikkonen *et al.,* 1997). Similarly the prominence of edge features is useful in archaeology, where the ability of microwave at certain wavelengths to penetrate overburden is of value. The detection of linear features is important in geological as well as geomorphological interpretation. "The physical features expressed in SAR imagery are directly related to structural geology (e.g., faults, synclines/anticlines), extent of lithological unit both in arid environments... and in tropical environments." (Brown *et al.*, 1996, pg. 412). The detection of linear features related to geology is often done manually and in conjunction with ancillary data such as Thematic Mapper data and geological maps (Rowan and Bowers, 1995).

While there is established value in the various microwave image products, there are also shortcomings. The principal shortcoming, when compared with other remotely sensed products coming from Thematic Mapper (TM) and other multi-spectral sensors, is that there is generally only one layer of imagery. For this reason, a large number of classifications are done using ancillary information such as obtained from ground surveys or data gathered from other sensors. Further, most recent active microwave research is concerned with the enhancement of RADAR imagery by its combination with other image data in a process known as "data fusion".

Generally, work in the area of data fusion centres around combining the spectral resolution of multi-spectral scanners with the spatial resolution of SAR imagery. A number of authors have claimed to have attained a degree of synergy by using various algorithms to fuse sensor products. Saint-Jean *et al.* (1995) employed Intensity-Hue-

Saturation (IHS) integration to combine C-Band SAR data with Landsat TM-5 imagery. In using this method, detailed on page 20, he claimed better results in classifying geological, hydrological and structural features than would be achievable with either product separately.

Although most work in data fusion is concerned with achieving apparent increases in spectral and spatial resolution, there are other fusion processes that merge images of similar spectral and spatial depth. Shimabukuro *et al.* (1998) employed two methods to fuse standard mode RADARSAT imagery from differing beam positions. First, the different beam position images were corrected to the same datum and viewed as red-green-blue components of a colour image. Second, Principal Component Analysis (PCA) was employed on the unfiltered and speckle filtered input images to provide input to a Martin Taylor Enhancement (see page 21). Similarly multiple beam angle composites have been used to classify macrophyte stands in tropical reservoirs (De M. Novo *et al.*, 1998). Other 'same sensor' fusions have been employed in ground cover studies. Composite images consisting of RADARSAT standard mode imagery taken over a period of months were used to evaluate landcover dynamics in the Amazon (Kux *et al.*, 1998).

1.1 Research Goals and Objectives

An application which makes use of the texture and edge determination capabilities of microwave remote sensing is the classification of geological features. Here, RADAR imaging can be particularly cost-effective (because of the difficulties involved in conducting ground surveys) in areas of high relief. Unfortunately, in areas of high relief, the shortcomings of microwave data, in particular the effects of shadow, foreshortening, and layover, become evident. As these effects are due solely to the geometry of the terrain relative to the sensor, using multiple look angles, and hence, multiple geometries, can increase classification accuracy. This project will look at a data fusion approach to employing multiple look angles to improve the classification accuracy

of RADARSAT active microwave imagery in areas of high relief. Its goals are to produce a single image, using a minimum of ancillary data, that contains all the information present in the input imagery. The reason for using a minimum of ancillary data, and the interest in keeping the processing overhead to a minimum, is the belief that the usefulness of a process is enhanced by minimizing the cost of completing that process.

1.2 Thesis Structure

This thesis consists of six chapters. The first chapter introduces the topic of data fusion as it is applied to active microwave remote sensing. It further states the objectives and goals of this project and the reasons for those objectives and goals. The second chapter provides background information on the characteristics of the sensor used and how those characteristics affect the imagery obtained through the sensor. It also discusses methodologies used to fuse imagery together. Chapter three describes the data sources for this project and the area to be studied. The fourth chapter is concerned with the specific steps, and the reasons for taking those steps, to first fuse the imagery and then to assess the results of that fusion. The fifth chapter assesses the results of the fusion of the ascending and descending pairs with respect to the goals of the project. The sixth and final chapter summarizes the results and advances possible avenues of research with regards to improving those results.

Chapter 2

Technical Background

2.0 Introduction

This chapter first discusses the basics of microwave remote sensing, starting from the basic principles of RADAR and proceeding to the more specialized topics of Synthetic Aperture RADAR (SAR) and the sensor used in this project, the RADARSAT satellite. This discussion is followed by an overview of SAR image interpretation considerations. The chapter concludes with techniques applicable to the fusion of single band data sets of similar resolution as is the case with opposite look RADASAT image pairs.

2.1 RADAR

RADAR is the acronym for **RA**dio **D**etection **A**nd **R**anging. It employs the active sensing of microwave radiation in the wavelengths of 1mm to 1 meter. An active sensor being one that is both the source and the detector of the sensing energy. RADAR systems do not necessarily produce images; Doppler RADAR systems, such as the ones used to determine the speed of cars, are examples of non-imaging systems. What is common to all RADAR systems however, are the factors that impact the interpretability of the signal returns. What RADAR measures is distance and intensity. Distance is determined by measuring the time it takes for a broadcast signal to return, multiplied by the speed of light, and dividing by two. In the simplest case, where there is only one target and one pulse, it is relatively simple to process the return. However, a single pulse can reflect off a variety of objects within its beam and at a variety of ranges, producing a return signal with many 'peaks'. Further, a scanning RADAR will send out many pulses, the returns from which can interfere with one another.

The second aspect of RADAR data, intensity, is equally prone to

complication. Factors that influence the intensity of return are composition, size, texture, and angle of incidence to the surface(s) being scanned. The electrical characteristics of what composes the surface have a great impact on RADAR reflectivity. A measure of the electrical character of a surface is known as the *complex dielectric constant.* In the microwave part of the spectrum, water has a dielectric constant more than ten times greater than that of most natural materials (Lillesand and Kiefer, 1987). This means that the reflectivity of soil, rock, or vegetation is highly dependent upon the moisture content; wet objects reflecting better than dry ones. One question that arises, noting how well water reflects RADAR signals, is how does RADAR penetrate clouds? RADAR can penetrate cloud cover where visible light cannot because microwave wavelengths are much greater than the size of the individual water droplets in a cloud. The cloud behaves as a single object, reducing opportunities for scattering. Other good conductors of electricity, such as metal objects like bridges, are good RADAR reflectors and show up as bright areas in imagery. Good reflectors, presenting a number of faces to the incoming beam, show up well because there is a better chance that a face will be close to perpendicular to the beam. Clearly, all things being equal, a large object will reflect microwave radiation better than a small one, but the texture and orientation of the object is more important.

The apparent roughness of a surface is dependent upon the wavelength of energy being used. The Rayleigh *criterion* states that a surface is a diffuse reflector (rough) if the root-mean-square (RMS) height of the surface variation is greater than one-eighth of the wavelength of the sensor beam, divided by the cosine of the incidence angle (Alaska SAR Facility, 1995). Since such surfaces reflect energy in all directions, a significant amount of energy makes it back to the antennae. It is important to note that the definition of a rough surface includes angle of incidence; hence what is 'rough' at one angle of incidence can be a 'smooth' or specular reflector at another. Another reflective process that increases the brightness of a 'surface' is volumetric scattering. This can occur in wet vegetation where RADAR pulses are reflected throughout the canopy eventually

exiting back to the sensor. A common mistaken assumption in the interpretation of RADAR imagery is that the signals penetrate the vegetation cover. This could only occur if the cover was exceptionally dry and the depth of cover was small compared to the wavelength of RADAR employed (Alaska SAR Facility, 1995).

Refraction occurs when microwave radiation is transmitted through a boundary between materials with different refractive indices. The beam 'bends' at the boundary and is ether transmitted, reflected, or absorbed (or a combination of these). For example a RADAR pulse may penetrate a cold, dry snow cover, be refracted at the surface, and then reflect off of, or be absorbed by, underlying wet snow, ice, soil, or rock; resulting in a combination of volume, surface scattering, reflection, refraction and absorption effects.

Specular surfaces reflect incoming energy away from the antennae at an angle equal to the angle of incidence. This means that a good reflector that would show up well if perpendicular to the RADAR beam, will not show up at all at other angles. An example of a good reflector behaving as a poor reflector because of this, is bodies of water.

The intensity levels detected by the RADAR receiver are also influenced by the polarization of the RADAR beam. A RADAR beam can be transmitted such that the microwave signal vibrates horizontally, vertically, or in a circular fashion. Similarly, a RADAR antenna can be tuned to receive signals horizontally, vertically or both. The possible variations used are HH (horizontal transmit, horizontal receive), HV (horizontal transmit, vertical receive), VV (vertical transmit, vertical receive), and VH (vertical transmit, horizontal receive). When a signal or portion thereof is changed from one orientation to another it is said to be *depolarized.* An application of a HV or VH setup might be to increase the variation between volume scattering objects and surface scattering objects. The multiple reflections and refractions occurring in volume scattering increase the amount of polarization that takes place relative to a scattering surface. An antenna that receives in a plane different from the transmitted signal will 'see' the

depolarized signal, in effect separating the two types of objects.

2.2 Synthetic Aperture RADAR (SAR)

The spatial resolution of RADAR imagery is dependent on the surface area of the receiving antenna, hence the large size of ground based tracking RADARs. This relationship to area is of particular importance in airborne or spaceborne operations where size and weight are penalized. To keep antenna size down, and at the same time increase resolution, airborne and spaceborne platforms take advantage of the fact that they are moving platforms to create a 'synthetic' antenna.

The two factors which determine spatial resolution in a radar system are pulse length and antenna bandwidth. Pulse length, or the duration of each microwave burst determines range resolution. The slant range resolution is equal to one half the pulse length and is independent of slant range. Ground range resolution, or pixel size in the range dimension, because it is dependent on angle of incidence, increases with distance from the sensor platform. Antennae bandwidth, or effective width of the microwave beam, determines azimuth resolution. This bandwidth is directly proportional to pulse wavelength and inversely proportional to antennae length. The effective bandwidth increases with distance as the beam spreads out. Brute force, or real aperture systems, depend on the physical antenna width to determine resolution. Synthetic aperture systems employ Doppler principles, data recording techniques, and auxiliary data processing, to simulate a large antenna, thus attaining high resolutions with a small antenna.

2.3 Interferometry

Interferometry uses the complex data set containing the **I** (In-Phase or real component), and **Q** (Quadrature, imaginary component) to accurately determine the *phase* of a particular return. If an object is imaged from the same point on two separate occasions and the phase of the return differs, then the object must have moved. Similarly,

if a stationary object is imaged from two locations, the phase difference can be used to determine the objects height. This allows complex SAR data sets to be used in seismology, or to generate Digital Elevation Models (DEMs). The accuracy with which distances can be determined using interferometry allows for the mapping of bottom features based on the effect bathymetric relief has on the surface of oceans.

With the launching of the RADARSAT sensor relief restitution by Radargrammetry is now possible using stereo image pairs instead of interferometry. The problem with interferometry from images obtained in repeat passes, is that distortions are introduced due to atmospheric perturbations between passes (Marinelli *et al.*, 1997). The methodology using stereo RADARSAT pairs is similar to that used to create Digital Elevation Models with other types of stereo imagery. Pixels representing the same point in both images are identified, intermediate pixels interpolated, and relief calculations, based on differences in pixel position performed.

2.4 RADARSAT

RADARSAT is the first commercial orbital SAR system. Launched in 1995, it follows a near polar orbit crossing the equator at dawn and dusk. It orbits 14 times per day. Data are collected in a line parallel to the satellite track, offset to the right of nadir 250km. The image swath is a maximum of 505km. One consequence of this orbit is that the satellite passes over the earth's surface in two directions, ascending and descending, obtaining imagery from opposite sides. This is important in RADAR imagery, since the effects of foreshortening, layover, and shadow, as well as the various factors affecting intensity, are related to angle of incidence.

The RADARSAT satellite collects C-Band (5.6 cm) imagery at seven beam modes, Standard, Fine, Wide, ScanSAR Narrow, ScanSAR Wide, Extended Low, and Extended High (Figure 1). Standard mode has a 100 kilometer swath with a resolution of 25-28 meters. Fine mode has a 45 kilometer swath with 9 meter resolution. Wide mode has a resolution of 28-35 meters with a 150 kilometer swath. ScanSAR and

the extended modes are combinations of the first three modes. ScanSAR Wide uses two Standard swath and two Wide swath beams. ScanSAR Narrow uses three Wide swath beams. Wide ScanSAR has a 500 kilometer swath at 100 meter resolution while ScanSAR narrow has a 300 kilometer swath at 50 meter resolution. The two final beam modes are Extended High and Extended Low. There are six Extended High mode beam positions starting 750 kilometers off nadir and extending out to a range of 1175 kilometers. The three inner Extended High mode swaths are a nominal 80 kilometers wide and the three outer swaths are a nominal 70 kilometers wide. Extended Low mode is a swath 170 kilometers wide centered 250 kilometers off nadir.

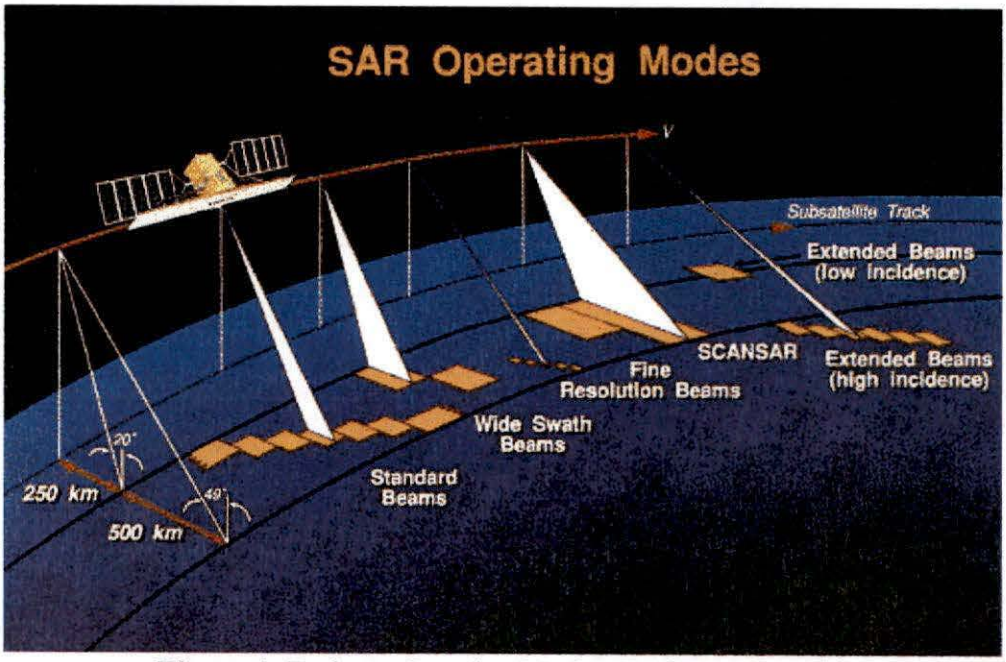

Figure 1. Radarsat Imaging Modes (Radarsat Canada)

2.5 SAR Image Enhancement

To aid in SAR image interpretation there are a number of enhancements and corrections commonly made previous to classification. First of these is speckle removal. The coherent nature of RADAR waves causes random constructive and

destructive interference resulting in multiplicative noise, or speckling, in the imagery (Lillesand and Kiefer, 1987). Since the noise is random there is no way to differentiate, with absolute assurance, between noise and information or, be sure of what information the noise is obscuring. However, some attempt at speckle removal must be made, and this has been the focus of much research in the field of SAR interpretation. Methods of speckle removal include multiple-look processing. Here, multiple images of the same area, using different portions of the synthetic aperture, are averaged, producing a smoother image. The problem with this method is that the resulting resolution is inversely proportional to the number of looks used. Using four images decreases resolution by a factor of four and decreases speckle by a factor of two. This means that the decrease in speckle is gained at the cost of resolution. Another technique forwarded does not use different looks of the same acquisition, but utilizes images acquired at different times. Here it is claimed, "...it allows for the reconstruction of the underlying radar reflectivity time evolution at the full spatial resolution of the signal but with a dramatic improvement of the signal to noise ratio..." (De Grandi *et al.*, 1997).

Another more common and less computationally complex method of speckle removal employs the use of simple filters, such as median and averaging filters. Other speckle specific filters have been developed including the Lee, Kuan, Enhanced Lee, Frost, Enhanced Frost, and Gamma MAP filters, all based on local variance statistics. These methods trade off speckle removal with the preservation of useful information. Another, more complicated approach, employs multi-resolution filter banks and discrete wavelet transforms to remove speckle and preserve information (Sveinsson and Benediktsson, 1997).

Other impediments to SAR image interpretations are the effects of foreshortening, layover, and shadowing; the impact of these effects increasing with the relief of the area to be classified (Alaska SAR Facility, 1995).

In the following three illustrations, θ is the angle between the imaged surface and the earth spheroid, a is the lowest point on the surface, b is the highest point,

and a' and b' are the SAR images. Foreshortening occurs when, as the angle θ increases, the range to point b from the antenna decreases, relative to point a. For all positive angles θ, this results in the observed distance $a'b'$ to be less than the ground distance ab (figure 2). Angles θ, greater than a particular angle produce a ground image where the positions of a and b appear reversed, a layover situation (figure 3). Shadowing occurs when the path of the microwave beam is blocked by an obstruction, similar to the shadows occurring using visible light (figure 4).

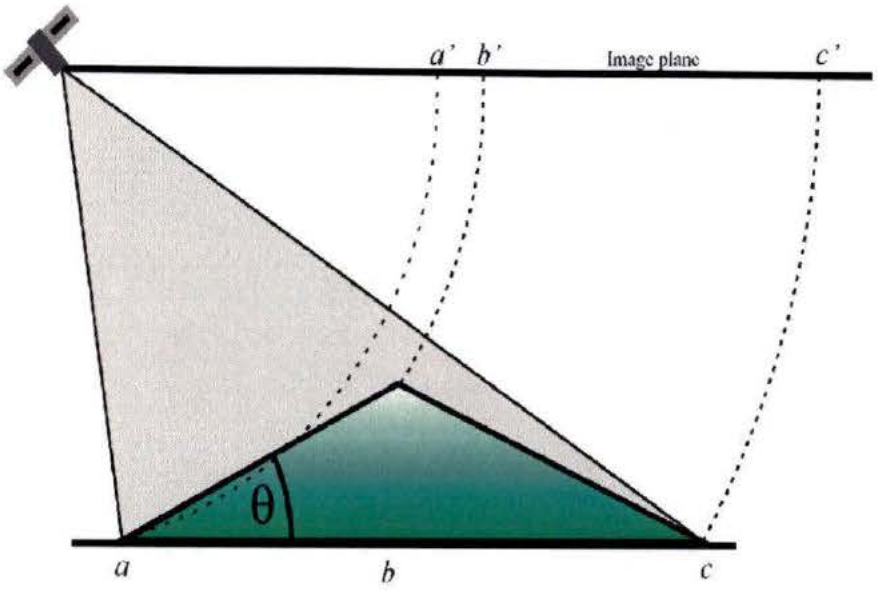

Figure 2. Foreshortening

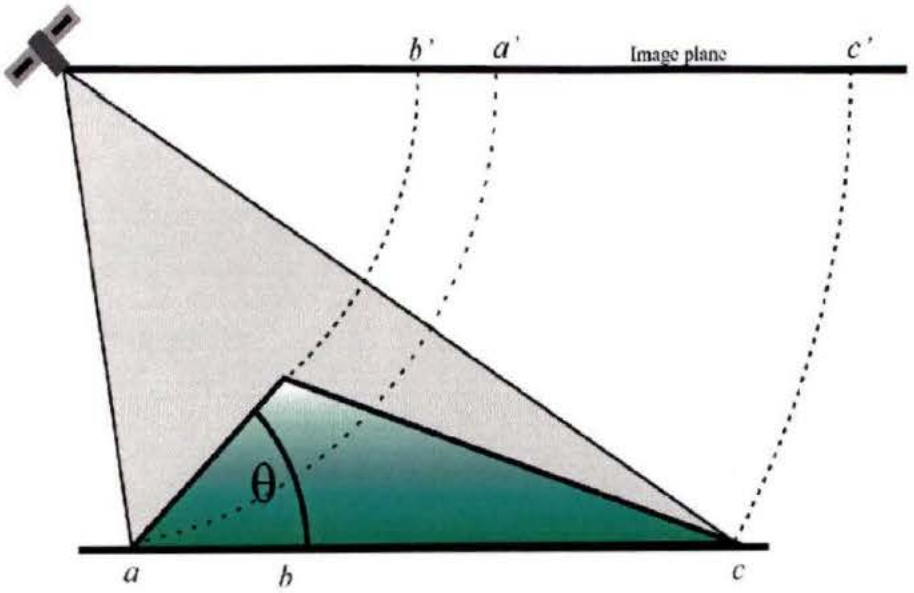

Figure 3. Layover

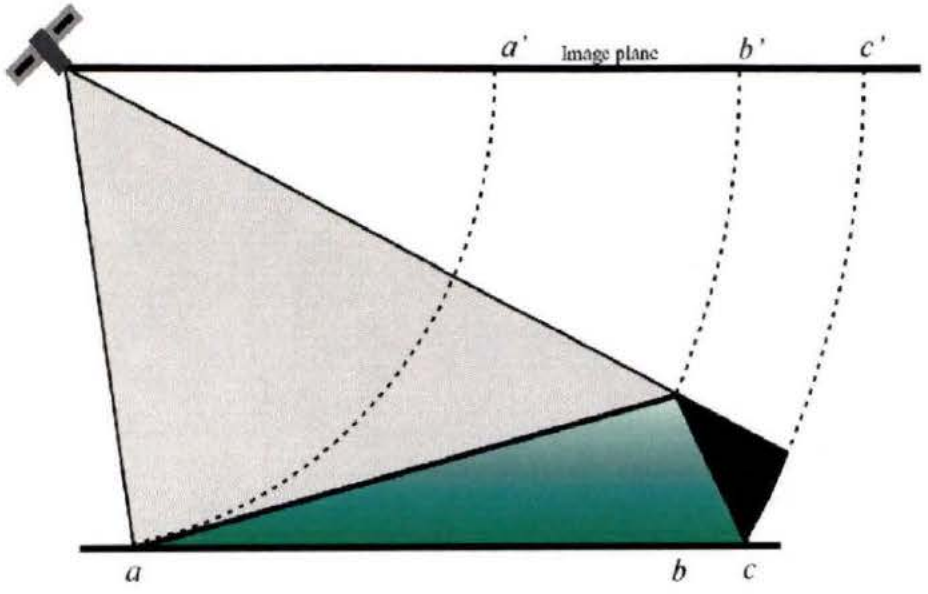

Figure 4. Shadowing

The most straightforward means of decreasing the impact of geometry on SAR imagery is to chose acquisition angles, or in the case of RADARSAT imagery, beam modes, that reduce these effects (Singhroy, 1997). For example, incidence angles of 40-59 degrees were found to be the least problematic for structural and geomorphic mapping. In mapping Precambrian shield terrain Singhroy found angles of 20-31 degrees to be suitable while angles of 25-45 degrees were best for rolling terrain.

Given that there is a problem with relief effects, the interpreter can either mask out the areas of layover and shadow, or try to rectify the image, removing the effect. In both cases, a digital elevation model is used. Little can be done to estimate backscatter in areas of layover and shadow, and so a mask is required to mask out such areas (Pairman and McNeill, 1997). D. Pairman and S. McNeill propose an algorithm for finding these areas that does not involve converting the image back to the slant range domain as others do. They claim this simplifies processing, and assume constant bearing to the satellite among other constants to further simplify the process. In contrast to this simplified approach some practitioners use a DEM to create a synthetic SAR scene which is used to determine layover/shadow areas (Gelautz *et al.*, 1997).

2.6 Data Fusion

Data fusion techniques are usually applied to improve the apparent spatial resolution, or spectral depth, of a data set. An example is the use of Intensity-Hue-Saturation (IHS) methods to fuse 'System Pour L'Observation de la Terre' (SPOT) 10 metre High Resolution Visible (HRV) data sets with 20 metre SPOT multispectral data. This is done to increase the apparent spatial resolution of the multispectral data set (Franklin and Blodgett, 1992). Other fusion techniques attempt to combine data sets that are spatially similar but differ spectrally or temporally. An example of this is the visual enhancement of deforested areas in Brazil through the combination of wet and dry season RADARSAT imageries. Here, the images are viewed as red, green, and blue components

of a colour image (Shimabukuro *et al.*, 1998).

The techniques used to achieve this information fusion range from simple arithmetic methods to complex wavelet transforms. The most common methodologies are, in order of complexity:

- Band Substitution
- Arithmetic
- High Pass Filter
- Principal Component Analysis
- Intensity Hue Saturation
- Radiometric
- Statistical
- Spherical Coordinate
- Wavelet Transform

Band (or component) substitution is simply a colour composite using the high spatial resolution band as one of the RGB components. For example, Thematic Mapper bands two and three may be displayed as green and red respectively, while blue is determined by the higher resolution SPOT panchromatic imagery (Vrabel, 1996).

In an arithmetic combination the value of each output pixel is determined by a function of the corresponding pixel values in each of the input bands. This can be simple, such as a weighted addition of bands, or complex, such as a Colour Normalized (CN) transform. In a CN transform of SPOT and TM imagery, the three visible TM bands are multiplied by the SPOT panchromatic band and then normalized by the following equation (Vrabel, 1996):

$$CN_i = \frac{(P_i + 1.0) * (PAN + 1.0) * 3.0}{(\sum_i P_i + 3.0)} - 1.0$$

where P_i is the multispectral imager band pixel value, PAN is the SPOT (in this case) pixel value and CN_i is the output colour normalized pixel.

The High Pass (HP) filter transform is simply an arithmetic combination, with filtering applied to the input bands before the arithmetic function is applied. A high pass filter maintains the high frequency 'detail' information while smoothing the lower frequency information. A low pass filter performs the opposite operation, smoothing the more abrupt changes in image intensity. In the HP transform, a high pass filter is applied to the input high spectral resolution image, a low pass filter is applied to the lower resolution multispectral images, and the output value is the weighted sum of those filtered images (Vrabel, 1996).

Principal Component Analysis (PCA), by itself, is not commonly used in traditional data fusion. It is normally used to reduce a number of data sets into a smaller, more easily manipulated, set of images. Since it is performed on image sets of equal pixel resolution, it has limited appeal as a data fusion technique where the data sets are generally of dissimilar spatial resolution. It will be discussed in some detail here however, because it is a major part of the data fusion process employed in this study.

In digital remote sensing, data are generally presented as a number of images; each image representing the same area, but a different spectrum of light. These data sets, if closely spaced in the spectral domain, may have a high degree of correlation, and hence redundancy. The aim of principal component analysis is to generate new data sets that are uncorrelated and have certain ordered variance properties (Jensen, 1986). To accomplish this, a new set of axes is generated such that the first axis is associated with the greatest amount of variance in the scatter plot. The second axis, orthogonal to the first, contains the second most variance and so on. At most, *n* new axes can be created for *n* input images. The mechanics behind this transformation are illustrated in the following three figures.

A scatter plot of two highly correlated bands, the simplest case, might resemble figure 5 with band mean values μ_{band1}, and μ_{band2}. In figure 6, a new coordinate system is created such that Band1' = Band1 - μ_{band1}, and Band2' = Band2 - μ_{band2}.

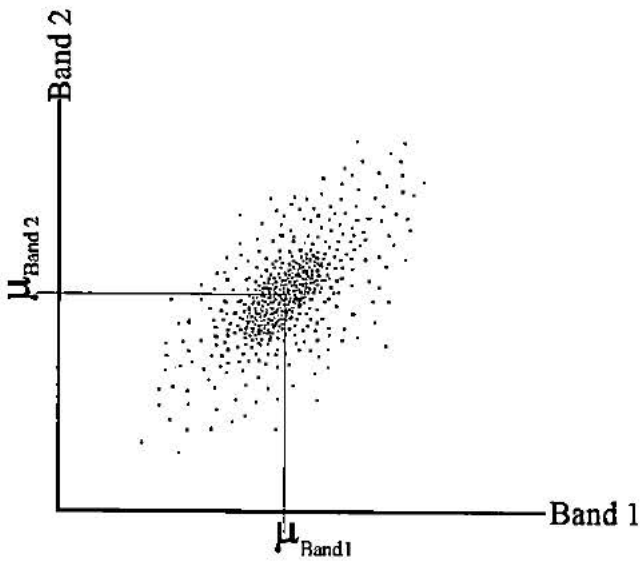

Figure 5. Two Band Scatter Plot

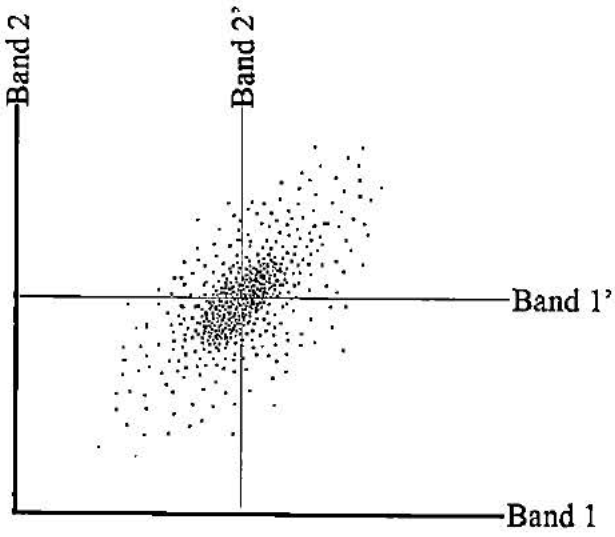

Figure 6. Transposition of Axes

In Figure 7 the axis has been rotated about the new origin (μ_{band1}, μ_{band2}) such that the first principal component axis (PC1) is projected through the semi-major axis of the point distribution and the second axis (PC2) is at a maxima and remains

perpendicular to the first. The first principal component, therefore, contains the majority of the variance present in the two data sets and is uncorrelated with the second principal component. Typically, in the case of Thematic Mapper data, the first principal component contains approximately 90% of the variance in the data sets (Jensen, 1986).

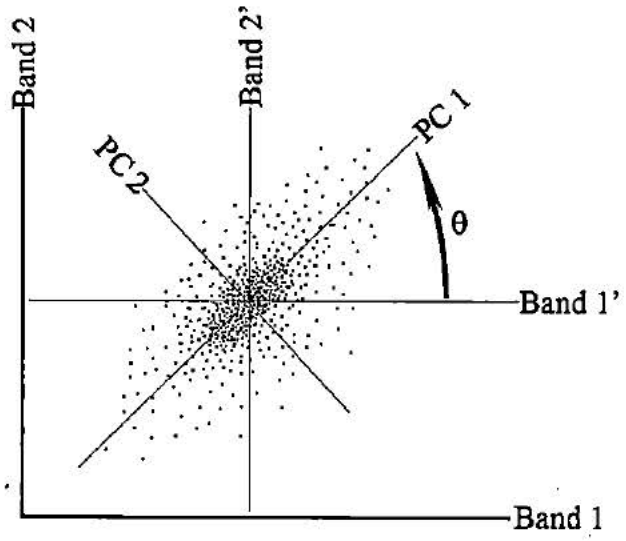

Figure 7. Rotated Axes, First and Second Principal Components

Mathematically, the computation required to transform the original pixel values to the principal component images looks like:

$$PC_{i,j,p} = \sum_{k=1}^{n} EV_{k,p} BV_{i,j,k}$$

where

$PC_{i,j,p}$	Brightness value in pth principal component image for pixel at row i column j
$EV_{k,p}$	Eigenvector for pth principal component for band k
$BV_{i,j,k}$	Brightness value in band k image for pixel at row i column j

The Eigenvector matrix EV is derived from the covariance matrix such that:

$$EV_{[nxn]}Cov_{[nxn]}EV^{t}_{[nxn]} = E_{[nxn]}$$

where

$EV_{[nxn]}$	is the eigenvector matrix for n image bands
$EV^{t}_{[nxn]}$	is the transpose of the eigenvector matrix
$Cov_{[nxn]}$	is the covariance matrix for the n bands of remote sensing imagery to be transformed
$E_{[nxn]}$	is the eigenvalue matrix such that the elements (λ_{ii}) of the diagonal are the variances of the ith principal component. All non-diagonal members are zero.

From this equation two important values may be derived. First, is the percentage of total variance explained by a particular principal component p.

$$percent_p = [\frac{(\lambda_p)}{(\sum_{k=1}^{n} \lambda_k)}] \times 100$$

where

$percent_p$	percentage of total variance explained by principal component p
λ_p	is the pth eigenvalue (component)

Second, are the factor loadings, or correlations, between each of the input bands and the computed principal components. The calculation for determining the correlation of each band k with component p is:

$$Correlation_{k,p} = \frac{A_{k,p} \times \sqrt{\lambda_p}}{\sqrt{Var_k}}$$

where

$Correlation_{k,p}$	is the correlation of band k with component p
$A_{k,p}$	is the eigenvector for band k and component p
λ_p	is the pth eigenvalue (component)
Var_k	is the variance of band k in the covariance matrix.

The most common fusion transform based upon Principal Component Analysis, and the basis for a number of other fusion methodologies, is the Intensity Hue Saturation (IHS) transform. The basic principle here, is that the multispectral bands are transformed into a coordinate system where one of the axes represents intensity. This intensity axis is replaced by the high spectral resolution image, and the system is transformed back into the original coordinate system. For example, three bands (i.e. Red Green Blue) of a low spatial resolution data set, are transformed into IHS space. The intensity component is then replaced with a higher resolution image which has been contrast stretched to match the variance of the intensity component. The IHS components are then retransformed back to the original spectral space retaining the higher spatial resolution of the replaced intensity image. The details of the transform to the IHS space are (Pellemans *et al.*, 1993):

P_i (i =1,2,3) are the pixel values of the multispectral bands

$$Intensity = \frac{(P_1 + P_2 + P_3)}{3}$$

$$Hue = \arctan\left(\frac{(2P_1 - P_2 - P_3)}{(\sqrt{3}(P_1 - P_3))}\right) + C$$

where $C = 0$, if $P_2 \geq P_3$

$C = \pi$, if $P_2 < P_3$

$$Saturation = \frac{\sqrt{6}}{3}\sqrt{(P_1^2 + P_2^2 + P_3^2 - P_1P_2 - P_1P_2 - P_2P_3)}$$

The first variant of the IHS data fusion technique utilizes Principal Component Analysis (PCA). PCA is performed on the lower spatial/higher spectral resolution data with the first principal component replaced with the higher spatial resolution image before retransformation back to the original space. The theory behind this is that the spatial information in the multispectral (low spatial resolution) band images is highly correlated, and thus will be held in the first principal component, while the spectral information will be held in the subsequent components (Chavez *et al.*, 1991). Another PCA based fusion technique is the Martin Taylor Enhancement (MTE). As the name implies, this is more of an enhancement than a data fusion methodology, as it is used on data of similar spatial resolutions. Originally, in the early 1970s, MTE was used on four band LANSAT MSS data to enhance its colour rendition, but it has been used more recently to enhance RADARSAT imagery. Here, the input bands have principal Component Analysis applied against them, and the first three component channels are interpreted as intensity, red-green, and blue-yellow (PCI, 2000). In the case of RADARSAT data, filtered and unfiltered images of two beam modes are used as input to

the PCA (Shimabukuro *et al.*, 1998).

In all of these IHS based transforms it is the intensity channel which is replaced to simulate a higher spatial resolution sensor. In the radiometric method, instead of using a relatively high resolution image such as SPOT panchromatic, the intensity channel is determined by functions which use the spectral sensitivity curves and calibration factors of both the high spectral and high spatial resolution images to generate a synthetic panchromatic channel. Since the radiometric method preserves absolute pixel values, the statistical assumptions that subsequent processes are performed under retain their validity. Further, this method is not restricted to three multispectral input bands as is a true IHS transform (Pellemans *et al.*, 1993).

The statistical method, as with the radiometric method, is not restricted to three input bands and attempts to maintain the original depth of image information. Instead of using sensor properties to derive an intensity channel, the statistical method aims to maximize the correlation between the simulated (synthetic) intensity channel and the panchromatic channel. This maintains the energy balance such that the average of the calculated intensity over the image is equal to the mean of the panchromatic image (Pellemans *et al.*, 1993).

The Spherical Coordinate transform derives intensity, the value which is to be replaced by the high spatial resolution image, from a conversion between the Cartesian coordinate system and the spherical coordinate system. Each RGB pixel in a Cartesian coordinate system has a position on each of three axes (Red, Green, Blue) as part of a three dimensional rectangular coordinate space. When converted to a Spherical coordinate system, each pixel is identified by two angles, (θ,ϕ) and a radius r. The value r can then be interpreted as the intensity component of the low spatial resolution image to be replaced by the higher spatial resolution image. After the replacement the system is converted back to the Cartesian coordinate system.

$$r=\sqrt{(P_1^2+P_2^2+P_3^2)}$$

$$\Theta=\arctan\left(\frac{P_2}{P_1}\right)$$

$$\Phi=\arctan\left(\frac{\sqrt{(P_1^2+P_2^2)}}{P_3}\right)$$

(Zwillinger, 1995)

The wavelet transform is an intermediate representation of signal information between a representation in the spatial domain, and a representation in the frequency domain (Yocky, 1995). The application of the wavelet transform to the problem of data fusion is an attempt to improve upon the results possible with the predominant IHS transform and its variants. The IHS methodologies replace one component of the spectral characteristics of an image with a higher spatial resolution image. This, on the assumption that there is a high degree of correlation between the input bands, so little information will be lost by replacing one highly correlated component with another. However, if the three input bands are not well correlated, as is the case in much of the imagery not in the visible range, then information is lost in the replacement of the intensity component (Vrabel, 1996). Methodologies such as the statistical and radiometric approaches to IHS transforms attempt to compensate for this information loss through the use of preprocessing and ancillary information. A wavelet transform fusion in contrast, seeks not to replace one component of an image with a higher resolution one, but to increase the apparent resolution of all input imagery. This is accomplished by first extracting the 'detail', or 'structure' information, in the high and low spatial resolution imagery, by use of a wavelet transform. This information is commonly taken in three directions, horizontally, vertically, and diagonally (Garguet-Duport *et al.*, 1996). The 'detail' present between the high and low spatial resolution images is then

inserted, by way of wavelet coefficients, into the low spatial resolution wavelets. A reverse wavelet transform is then performed to generate new high spectral/spatial resolution images.

As in the IHS transform and its derivatives, the standard multi-resolution wavelet decomposition (MWD) has problems. Small objects of a few pixels lose their spectral definition and the reconstructed imagery can contain artifacts in the form of ringing (Yocky, 1996). Variants of the MWD, developed to reduce these effects, are the additive, and selective, resolution wavelet merger techniques.

Chapter 3

Data Sources and Study Area

3.0 Introduction

This chapter describes the data used in this project. It begins with the source of the data in terms of who provided it and why. It concludes with the geographical location of the data, and why that location was chosen.

3.1 Study Area and Data Sources

On December 1st 1995 a project proposal by Eric Grunsky of the Ministry of Energy, Mines And Petroleum Resources – Geological Survey Branch was selected to receive data under the Application Development and Research Opportunity (ADRO) Program. The project title is "An Evaluation of Radarsat For Multi-disciplinary Geological Mapping In British Columbia", the ADRO project number is 151. The project objectives are;

> "To evaluate the usefulness of C-band SAR data at the local and regional scales for integrated geoscience projects.
>
> Attempt to develop a methodology for incorporating SAR data into areas of high relief for a more effective interpretation of geology and associated structures (Grunsky, 1995)."

The project proposed two study areas, a large regional study area and a local scale study area. The regional scale study area is the Nechako region of the Chilcotin Interior Plateau, part of the NATMAP Interior Plateau project which is a joint project of the British Columbia Geological Survey Branch, and the Geological Survey of Canada. The local scale study area is the Totagga Lake area in northern British Columbia (Figure 8).

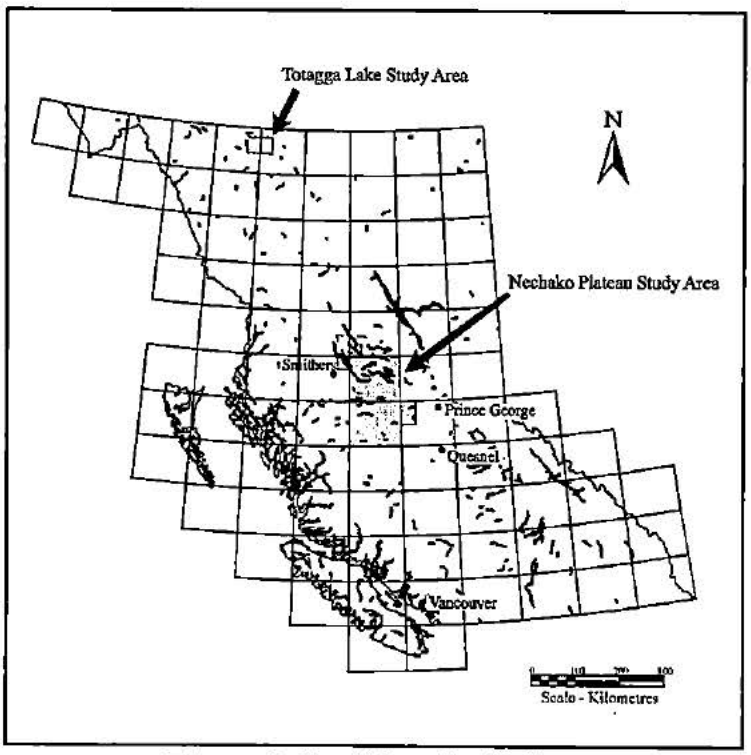

Figure 8. Candidate Study Sites

Through the ADRO project, RADARSAT imagery has been obtained consisting of opposing look angle pairs for two study areas in northern British Columbia. The Totagga Lake study area is covered by an ascending and descending pair of RADARSAT FINE 4 images obtained on October 8, 1996. Each image covers an area of about two thousand five hundred square kilometres, with the overlapped area being less than eight hundred square kilometres, and centred at approximately 57° 45'N/129° 55'E. The area is characterized by well defined slopes and ridges. Elevation in the area ranges from 2694 feet at Kinaskin Lake to 6553 feet at Todagin Mountain. The Nechako Plateau study area pair consists of STANDARD 7 images of about ten thousand square kilometres acquired on August 30, 1996. The overlapped area for this pair is less than one thousand five hundred square kilometres, and is centred at approximately 55° 5'N/126° 30'E. The area is characterized by weathered, rounded surfaces. Elevation in the area ranges from 2332 feet at Babine Lake to 5148 feet at Old Fort Mountain. In

addition to the RADARSAT data, a Digital Elevation Model has been provided by the Geological Survey of Canada covering the overlapped area of the more northern SAR pair.

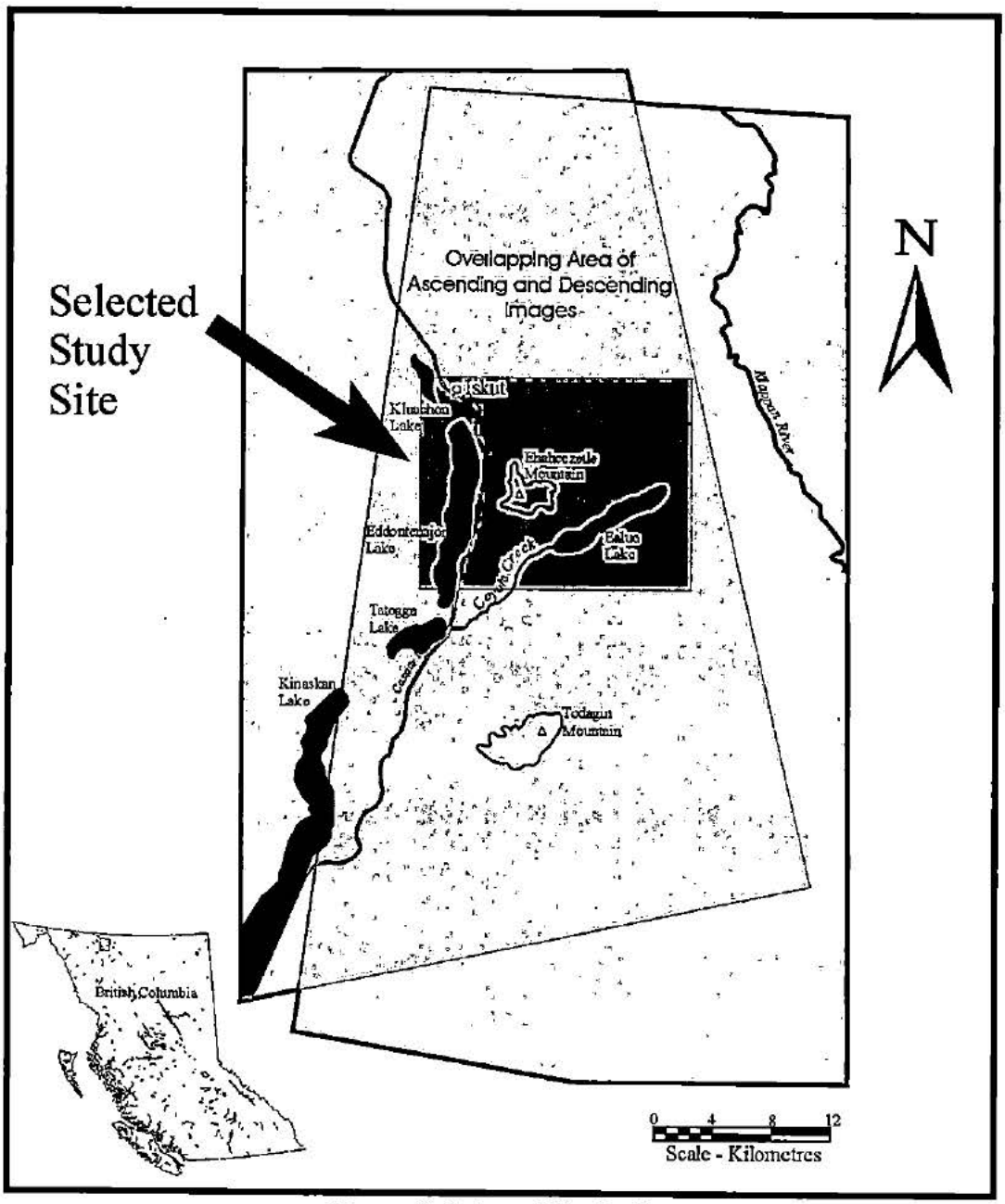

Figure 9. Selected Study Site

Of the two study sites, the Tatogga Lake site contains more sharply defined features, steeper slopes, and a greater variety of terrain types. For this reason, and because digital terrain data has been provided for this site, it was decided to proceed with the image pairs covering the more northern Tatogga Lake site (Figure 9). Water feature and ridgeline data for this site in the form of vector files from the Terrain Resource Information Management (TRIM) project were obtained from the Ministry of Environment Lands and Parks through Barrodale Computing Services Ltd. Thirteen 1:20000 TRIM mapsheets were also obtained, completely covering the overlapping area of the two RADARSAT images.

Finally, a Thematic Mapper mosaic of bands 2, 3, 4, and 5, at 50 metre resolution was obtained. The mosaic completely covers the study area and is composed of Thematic Mapper images taken September 21, 1995 and July 23, 1994.

Chapter 4

Methodology

4.0 Introduction

This chapter discusses the processes employed to first create the product imagery, and second, to assess the quality improvement attained with respect to image classification. It begins with a characterization of the desired end product with respect to the goals of the project. Secondly, it discusses the constraints on possible fusion methodologies due to the nature of the input data and the proposed final product. It then describes the steps taken to arrive at the finished product, and the reasons for taking those steps. Finally, it describes the procedures used to assess the fused imagery.

4.1 Characterization of Fused Imagery

The stated goal of this project is to produce a single image, using a minimum of data ancillary to the RADARSAT imagery, that contains the identifiable features present in either input image. Of particular interest to this project are those features that manifest themselves particularly well in SAR imagery. Those features being lineaments, slope changes, and variations in surface texture. The information available in the output imagery should be available at the same scale as the input imagery. This, in recognition that high spatial resolution is an important feature of the sensor. The output imagery should also be geocorrected such that data from other sources, such as hydrological information, can easily be added. Finally, the process should not require the use of a Digital Elevation Model (DEM). Since much of the information hoped to be gained through the fusion process would be available in a DEM, using a DEM to facilitate the process would be redundant.

Counter to the characteristics of SAR imagery that we wish to maintain or

enhance, there are characteristics that we wish to reduce or remove. The characteristic that has the greatest negative impact on the interpretability of SAR imagery, in areas of moderate to high relief, are the effects of layover, foreshortening, and shadowing. In particular, the terrain features on foreslopes are distorted much more than on the backslopes. For example, with a look angle of about 20°, a foreslope of 10° will be foreshortened by a factor of .18, whereas the backslope will be foreshortened by a factor of .51 (Wivell *et al.*, 1993). As the slopes approach 20°, as they do in the project study area, the differences are even greater, and compounded by the high backscatter intensity of a facing slope. For these reasons, as much as is possible, the fusion technique used should not replace backslope information with foreslope information.

4.2 Constraints on Methodology

4.2.1 Constraints on Fusion Methodology

The determination of a methodology for the fusion of the two opposing look RADARSAT images starts with a process of elimination. Those established methodologies which cannot satisfy the goals of the project are identified and eliminated.

Data fusion methodologies are typically applied to data sets from different sources. Further, these methodologies are commonly used in 'band sharpening', the fusion of data sets of dissimilar spatial and spectral resolution (Vrabel, 1996). These data sets are commonly characterized by differing spatial, spectral, or temporal properties. However, in the case of opposing look angle SAR imagery the two data sets are the same, spectrally and spatially, and have insignificant temporal differences. Data fusion algorithms that combine multispectral and high spatial resolution panchromatic imagery, such as IHS, Radiometric, and Spherical Coordinate methods, have no application in this project since there are only two input bands, and they are of the same resolution. That still leaves a number of possible fusion processes that can be used on opposing look SAR image pairs. The simplest of these are the arithmetic methods.

An example of an arithmetic methodology applied to SAR imagery is described in a paper by Charles Wivell *et al.* (1993) where opposing pair ERS-1 data are merged to lessen the effect of foreshortening, speckle and shadowing. Here, a two step fusion process is employed. The images are compared pixel by pixel with the lowest of the two values assigned to the fused image. This selects backslope values over the brighter foreslope values. Secondly, to reduce speckle and the effect of shadow, the closest pixel value to the modal of the joint histograms is used in the output image (Wivell *et al.*, 1993).

Other methods of data fusion applicable to SAR data include wavelet and fourier methods. The argument against using these methods in this project is that it has been found that arithmetic and fourier/wavelet methods on their own require precise geometric corrections to produce satisfactory results (Yocky, 1995). The problems associated with the geometric correction of SAR imagery are described in the following section.

4.2.2 Constraints on Geometric Correction

In addition to the need to geometrically correct the imagery to allow for its fusion, the goals of the project require geographic registration of the SAR imagery so that it can be integrated with other digital data, such as rivers and roads. The process of collecting control points and performing a geometric correction is reasonably straight-forward in nadir imagery. Examples of nadir imagery being that which is collected by Thematic Mapper and SPOT sensors. Methods that have been employed with nadir imagery include two-dimensional image transformations, and the use of manual photogrammetric techniques. Local distortions in off nadir SAR imagery, especially in mountainous areas, make the collection of control points and subsequent geometric correction a more complex process than in the nadir case. Two dimensional transformations of SAR imagery are fundamentally limited by their inability to handle the localized distortions caused by relief. Current methodologies use digital elevation models

to geocode SAR imagery, producing more accurate geocorrections with fewer control points (Toutin *et al.*, 1992). In addition, techniques have been developed to automate the collection control points with the aid of DEM's (Gelautz *et al.*, 1997).

While the margins of error attained by Toutin, Gelautz and others would be acceptable for this project, that accuracy is dependent upon the utilization of a DEM, the use of which has been excluded. Excluding the use of a DEM leaves the possibilities of correcting of both input images to each other, or to ancillary control points. In either case, as seen in figures 10 and 11, finding control points common to the ascending and descending images is complicated by the fact that features such as slope breaks may not be apparent in both images.

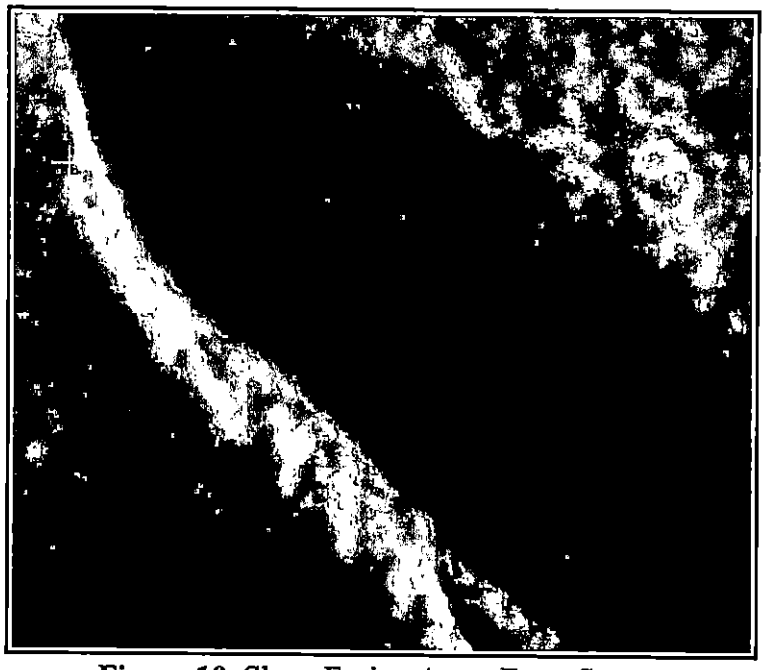

Figure 10. Slope Facing Away From Sensor

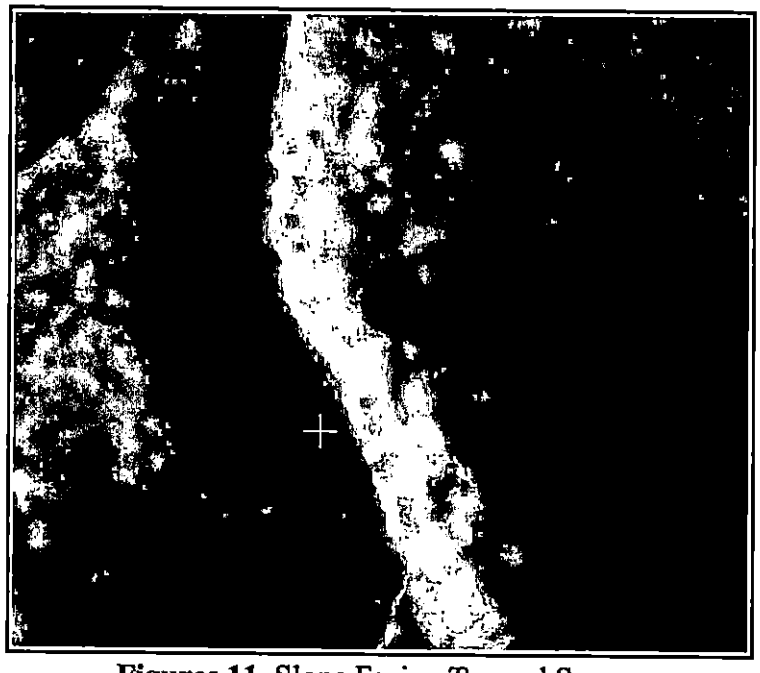

Figures 11. Slope Facing Toward Sensor

The exclusion of DEMs in the geocorrection process means that more control points will be required to attain the desired accuracy than would be necessary if a DEM was used (Toutin *et al.*, 1992). How many control points need to be found depends upon the scale at which the imagery is to be viewed, and the algorithm used to fuse the imagery. As has been mentioned, arithmetic and fourier/wavelet methods are sensitive to images that are not precisely geometrically corrected to each other. The degree to which the fusion methodology determines the number of control points required, is demonstrated in figure 12. The images in the figure are the result of two input images merged with two different arithmetic algorithms. The factors used in these equations were derived experimentally and simply serve as an example of how different image merging techniques impact the precision requirements of employed geometric corrections. The image on the left is a scaled average of the two input images;

$$merged\ value = \frac{(1.0 * input\ image_1 + .5 * input\ image_2)}{2}$$

The image on the right is a scaled difference of the two input images;

$$merged\ value = 1.0 * input\ image_1 - .5 * input\ image_2$$

The appearance of 'twinned' rivers in the scaled difference image, that are not apparent in the weighted average image, demonstrates that an geometric correction of acceptable precision for one fusion technique may not be acceptable for another.

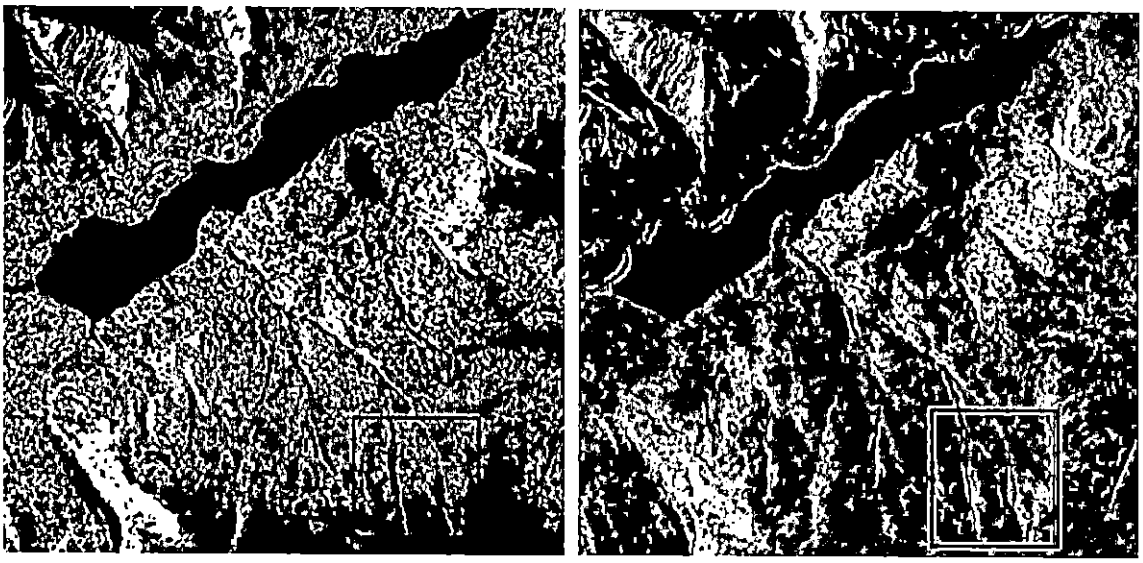

Figure 12. Impact of Fusion Methodology on Control Point Selection

4.3 Terrain Classification by Image Texture

Image classification by texture differs from spectral classification in that textural features are identified through the spatial variation of tone in a single image whereas spectral classifications are concerned with tonal variation through multiple bands. In the classification of SAR imagery through the use of texture, four types of intensity variations must be considered (Dobson *et al.*, 1997). First, is the variation in average intensity between terrain types. Second, is the variation within terrain types due to spatial variance in geometry, as might occur with differing tree types. Third, is the variation within a terrain type due to temporal variance, as in changes in soil moisture. Fourth, are the random variations in intensity due to pixel fading (speckle). Since there is little temporal difference between the two input images, and most of the textural classification will be performed on speckle filtered images, the third and fourth points will not be considered here. Further, since the effects of shadow are a major consideration in this area of high relief, variation in average intensity between terrain types is inadequate as a classification critereon. This leaves local variations in intensity, what is most commonly thought of as 'texture', as the critereon used to classify terrain

cover.

In flat terrain, with a pixel resolution of approximately five metres, using multiple polarizations, classification accuracies approaching 70% have been attained in the determination of tree stand type, (pine, spruce, etc.) and age (Wilson, 1996). The pixel resolutions of this project's mono-polar imagery is six to ten metres. This would suggest that differences in texture between barren or sparsely vegetated exposed rock; or sand, water, and forested or heavily vegetated should be readily detectable. Due to its uniquely (in this scene) specular nature, water will be the most accurately classifiable. Sensor facing exposed rock and sand should also be easily classified. Where difficulties will arise is in the differentiation between barren and vegetated land. The problem areas are likely to be in areas of shadow, facing vegetated slopes, and broken barren terrain.

4.4 Lineament Detection

The aspect of SAR imagery of most interest to geologists is the ease with which lineaments can be detected in a scene. Manual interpretation of lineaments is by its nature subjective, and therefore, more objective, automated methods of analysis have been developed (Saether *et al.*, 1994 and Karnieli *et al.*, 1996). Among the algorithms employed to extract lineaments from an image are Fourier and Hough transforms where the data are moved from the spatial domain to frequency or parameter domains. In these domains, processing direction and collinearity are simplified. In the spatial domain the algorithms used generally employ several steps to determine lineaments (PCI, 2000). First, through the use of gradients, edges in the imagery are defined. This gradient image is then thresholded to create a binary edge image which is further manipulated to remove spurious edge segments and connect disjointed features.

In this project it is not so important that all detectable lineaments are found, but that certain types of lineaments are detected in all images. That is, as we are using lineaments as a measure of comparison, the lineament, if detected or missed in one image must, correspondingly be detected or missed in the comparison image. Since no

method claims greater precision than the others the spatial domain algorithm employed by the PCI software was used. Once the algorithm was chosen it remained to find the input parameters which created the most useful lineament map. Usefulness is defined as detecting lineaments which define the major features without cluttering the scene with spurious lines. The required parameters were determined through experimentation and applied on all images (see Appendix III).

4.5 Employed Methods

The data processing for this project, as outlined in the research objectives and governed by the constraints described above, took place in ten steps. These steps involve four distinct processes, speckle removal, geometric correction, image fusion, and image classification. Speckle removal was performed as a single computer operation on both input images. Geometric correction involved manual input to a computer process. The combination of the input images into a fused output product involved both statistical and arithmetic computer processes. Image classification utilized both subjective and quantitative methods. The quantitative methods employed software routines to classify areas of similar texture, and to detect lineaments in the input and output imageries. Subjective classification consisted of the visual interpretation of the input and output imageries.

The data processing steps, taken in order, were:

1) De-speckle the imagery to be fused
2) Geometrically correct the RADARSAT imagery to TRIM vector data
3) Apply geometric correction to unfiltered (speckled) imagery
4) Perform visual assessment of input imagery
5) Perform textural classification on unfiltered (speckled) imagery
6) Perform textural classification on despeckled input imagery

7) Perform lineament detection on despeckled input imagery
8) Fuse the imagery
9) Perform visual assessment of fused imagery
10) Perform textural classification on fused imagery
11) Perform lineament detection on fused imagery

4.5.1 Speckle Removal

This process reduces the noise inherent in SAR imagery through the use of algorithms that reduce the local variability of the data set, while retaining edge features. Algorithms commonly used for this purpose are Frost filters, Lee filters and their enhanced variants. The Lee filter employs ancillary information to adapt the algorithm to a particular image. Inputs to the Lee filter include the type of noise to be filtered, either additive or multiplicative (most radar noise is multiplicative). Noise variance can be determined either from sampling known 'flat' areas on the image or specifying the number of looks. The Frost filter, in contrast to the Lee filter, is an adaptive, damped convolution kernel whose members are determined using local statistics. The only ancillary data requirement (aside from filter size) is the damping factor, which governs the influence progressively more distant pixels have on the smoothing process (PCI, 2000). In keeping with the philosophy of this project that ancillary information requirements be kept to a minimum, the filter chosen for this step was the Frost filter. It was expected that larger matrices in the order of 7X7 and 9X9 would be used, as preliminary applications of the despeckle process showed that this level of smoothing produced an image with distinct features, at the scale desired. The determination of what constituted an acceptable number of distinct features, is discussed in the section on classification accuracy assessment.

4.5.2 Geometric Correction

The two options for geometric correction that met the criteria set for this project are a correction between images and a correction to ancillary control points. For two reasons the RADARSAT imagery was corrected to TRIM vector data. The first reason is, that by correcting the imagery to TRIM data, the final product will be similar in geometry to the images being used to evaluate the fusion process. Secondly, by using TRIM vector data, the choice of control points is not limited to only those features apparent in both input images. The warping technique used to geometrically correct the imagery was a thin plate spline. The thin plate spline model was used as an alternative to a high order polynomial correction as there was a need for the individual control points to be honoured. Further, thin plate splines are locally sensitive, unlike polynomial functions, so that corrections in areas of large local distortion (foreshortening) do not produce warping artifacts in other areas of the image.

4.5.3 Visual Assessment of Geometrically Corrected Input Imagery

One of the goals of this project is to increase the number of discernible features in the imagery. To show that an improvement in image classification had been made by combining the ascending and descending imagery three assessment methods were used. Two of the methods employed software algorithms to quantitatively assess the imagery. The third method was a subjective assessment through visual inspection. At this stage, the visual inspection was a comparison of the ascending and descending imagery with each other, to Thematic Mapper data, and to a shaded digital terrain model.

4.5.4 Textural Classification of Input and Output Imageries

It is beyond the scope of this project to perform an in-depth textural analysis and classification of the images in question. However, textural analysis can be used to support the contention that an improvement in the classifiability of vegetated and

non-vegetated areas has been achieved through the image fusion.

One means of assessing the image improvement achieved through an enhancement process is to compare classification accuracies before and after the enhancement. As mentioned previously, texture is a determinant of classification in SAR imagery. There are two concerns in this case with the use of texture to classify imagery. The first concern is the source of a ground truth of appropriate scale and detail. It has been asserted here that a reasonable classification of the RADARSAT imagery would differentiate between forested land and 'other'. The 'other' coverages are subdivided into water, barren, and rock/beach. Since Thematic Mapper data were available, taken within a couple of years of the SAR imagery, this was used as a source of ground truth. A simple, unsupervised classification of the Thematic Mapper imagery provided the four classes required. This does not constitute an absolute ground truth, but is adequate given the classification accuracy potential of the RADARSAT imagery in this study.

The second concern is the impact of speckle removal on the texture classification process. The literature recommends performing these classifications on imageries that have not been subject to speckle removal (PCI, 2000). However, in terms of general image interpretation, it is preferable that the imagery be despeckled. To determine if the fusion process improves the overall interpretability of the imagery texture, classifications at each stage of the fusion process will be performed. The results of the texture classification of the geometrically corrected unfiltered imagery will be compared to later textural classifications to ascertain whether an improvement had been achieved in the classifiability of the RADARSAT imagery.

The textural analysis was performed using the TEX procedure in the Radar Analysis package in the PCI software. The TEX procedure offers the option of employing a number of texture measures to an image. All these texture measures are based on the Grey Level Co-occurrence Matrix (GLCM) which describes the numerical relationship, fixed in direction and distance, between pairs of pixels in an image. Derived from this matrix is the Grey Level Difference Vector (GLDV) which contains the counts

of occurrences of absolute differences. These matrices can be used to quantify the levels of homogeneity, correlation or contrast in an image (PCI, 2000). The specific texture measure used in this project was the GLDV contrast measure which returns higher values in regions of greater local variance or contrast.

4.5.5 Lineament Detection on Input Imagery

For this project two digital classification methods were used, textural classification and lineament detection. It was originally intended that regions of similar slope and aspect be classified through density slicing, or some region growing algorithm. However, the large number of features detected and the dissimilarity between the input images made this test impractical. Lineaments will serve as a substitute test for slope regions, since most regions of similar slope are bounded by linear features such as ridges or valleys. This is especially true in this case because of the sharpness of the terrain.

Research into automated methods of classifying linear features is based on methods used in other gray scale imagery, such as aerial photos. These methods still require the intervention of a trained interpreter to extract the significant lineaments from the ones detected (Karnieli *et al.*, 1996). In addition, linear features that run orthogonal to the flight path do not show up as well as features that run parallel (Grunsky, 1995). These issues are less important in this case, as we are more concerned with the number of lineaments gained or lost in the fusion process than with the accuracy of those lineaments. Secondly, in both input images, with look angles separated by nearly 180° most linear features in the imagery run parallel to the sensor,.

The lineament detection algorithm used was that provided in the image processing suite of programs in the PCI software. This algorithm first generates a gradient image using an edge detecting filter. The gradient image is then thresholded, producing a binary edge image. From this binary edge image lineaments are generated through the combination, pruning and thinning of edges (PCI, 2000).

4.5.6 Image Fusion

Consideration of the constraints detailed previously in this chapter, led to the conclusion that the best means of merging the information present in both input images was to use a combination of statistical and arithmetic means. The statistical operations are best suited to determining which of the input images contains the greatest variance and hence, hopefully, least impacted by foreshortening, layover and shadow. Further through the statistical analysis some merging of local variance may be achieved. The arithmetic means are best suited to the merging of information regarding larger scale features as are defined by lineaments.

To perform the initial fusion, determine which image (ascending or descending) is less affected by foreshortening, layover, and shadow, and enhance the textural qualities of the imagery, a principal component analysis was performed on the despeckled and geometrically corrected input images. To bring the edge features from the two images together and to enhance the visual 'depth' of the output imagery, the slope faces from the ascending image were added to the first principal component through the use of image arithmetic and a bitmap.

The principal component analysis was performed using the PCA routine, in the multispectral analysis program suite, provided by the PCI software package. The image arithmetic was performed using the ARI routine, in the image processing program suite, provided by the PCI software package.

4.5.7 Data Flow Diagram

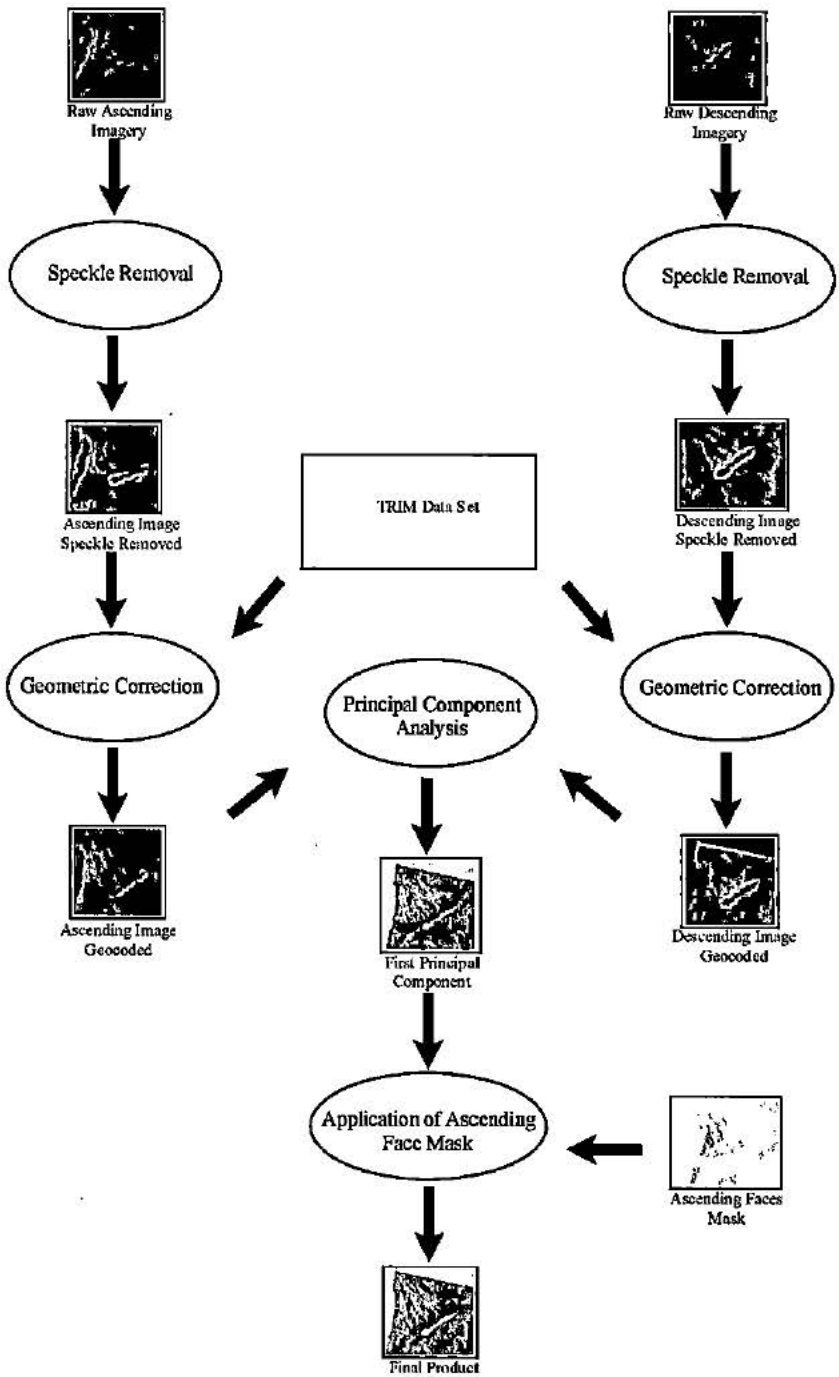

Chapter 5

Results

5.0 Introduction

This chapter details the application of the image fusion methodology. It first discusses the image improvement attained at each step of the fusion process. These discussions are subjective and focused on the required characteristics of the final product. It then looks at the results of the numerical tests employed; computer derived texture classification and lineament detection.

5.1 Application of Methodology

5.1.1 Geometric Correction

As explained in the methodology section of this thesis, the two input images must be spatially corrected to a common coordinate system before they can be fused. Here, the images were corrected to TRIM vector data in an UTM coordinate system. To aid in the identification of ground control points, and in later steps, image interpretation, the input images were filtered to remove the random noise inherent in SAR data (speckle). The speckle removal algorithm used was a simple Frost 9X9 filter. The results of the filter application are shown in figures 13 and 14.

One factor determining the utility of a particular image fusion technique is the cost of production. The greatest costs, in terms of time and computing resources, are incurred during geometric correction. The cost of geometric correction grows as the number of control points collected increases. This is because, as the number of remaining identifiable candidate control points in the imagery and vector data shrinks it takes longer to find them. Also, the amount of computing time necessary to correct the imagery increases non-linearly with the number of control points. Another complication, in this case and in general for SAR imagery, is that many control points are unique to a look

angle, some features not being discernible in both look angles. For these reasons, it is important to devise some test to determine when sufficient control points have been taken.

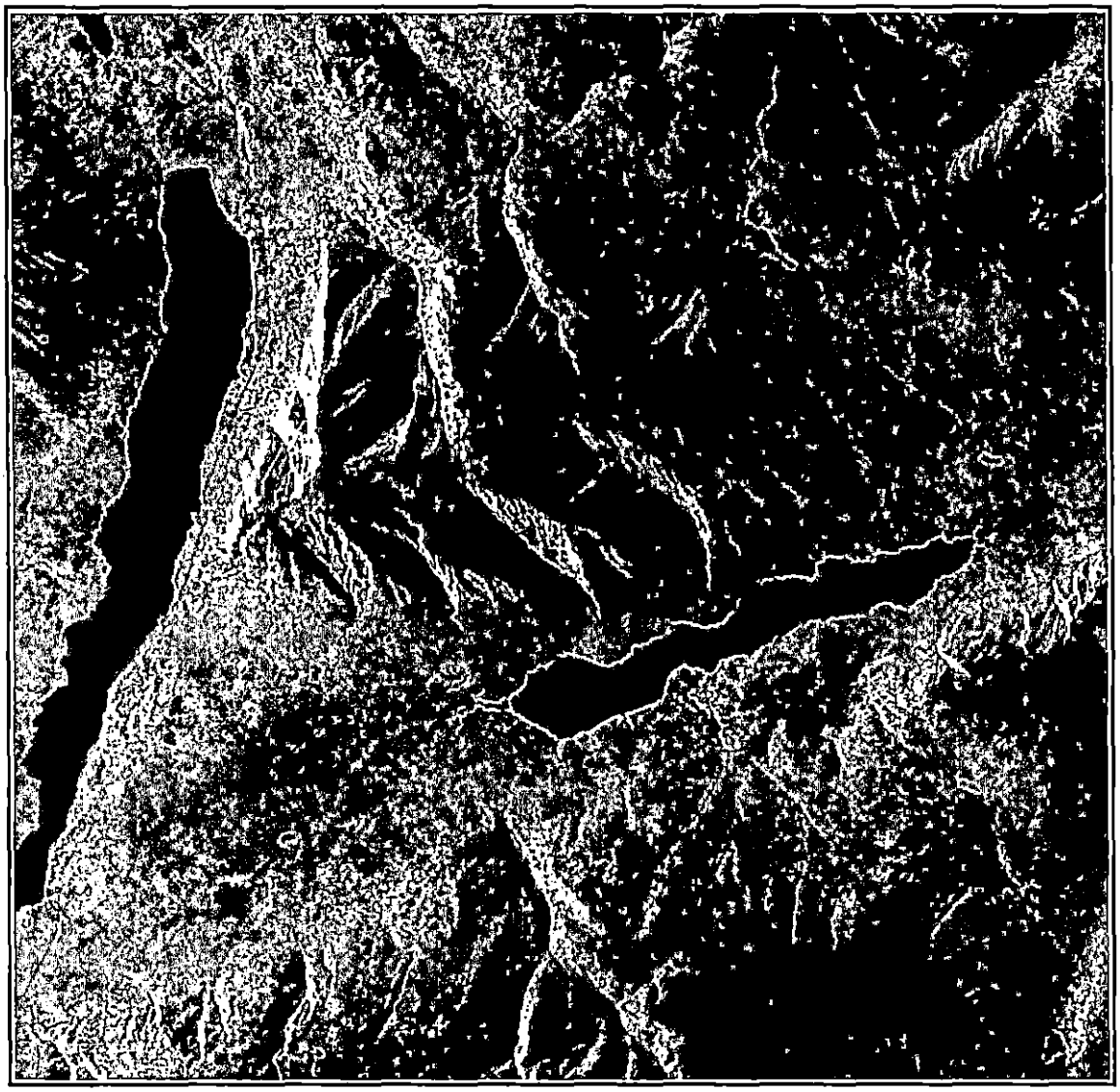

Figure 13. Ascending Imagery After Speckle Removal

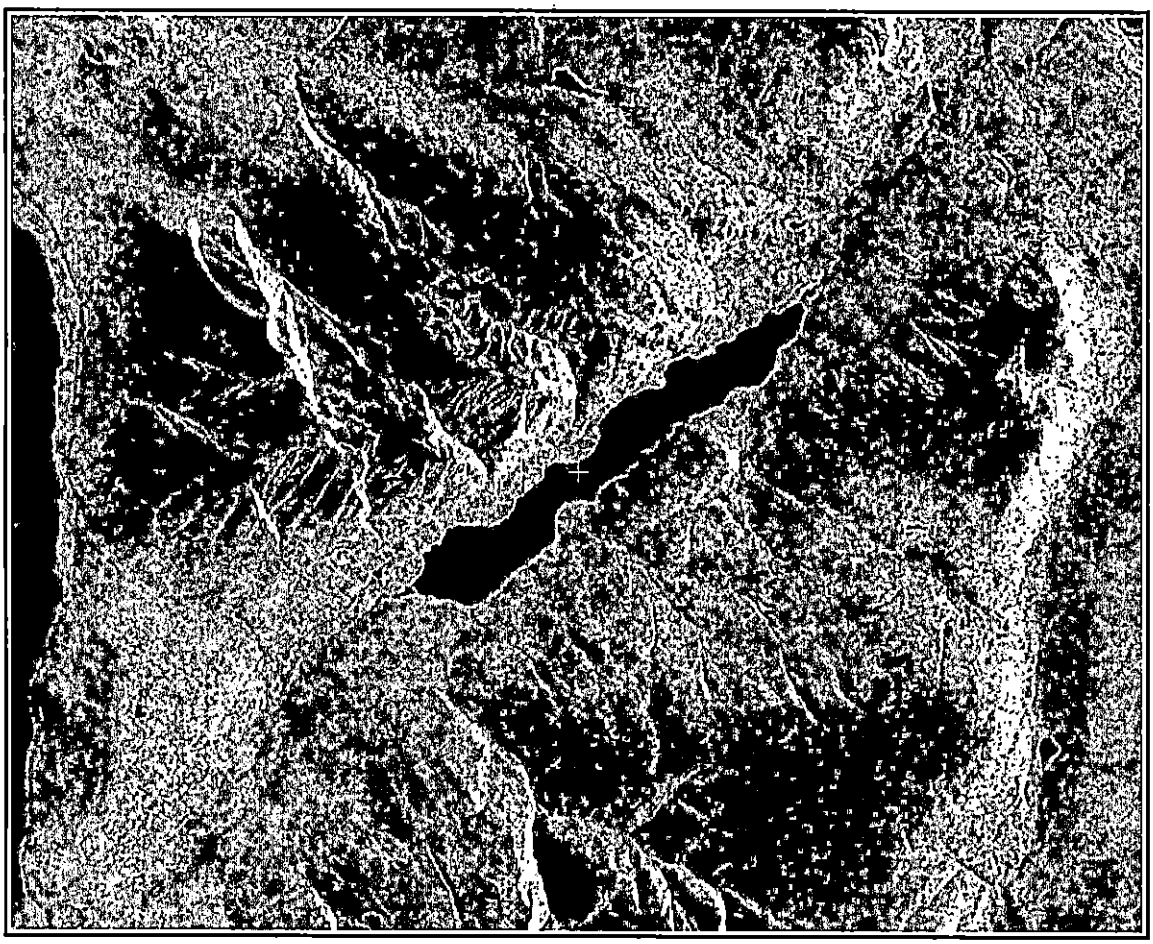

Figure 14. Descending Imagery After Speckle Removal

It was noted, that as control points on the two images were added, the amount of variance contained in the first principal component decreased. At twenty control points, the amount of variance contained in the first principal component was approximately sixty-eight percent (68%). At eighty control points, this had decreased to approximately sixty percent (60%). The rate of decrease slowed as points were taken, such that at one hundred and fifty points the amount of variance in the first principal component had not fallen below fifty-nine percent (59%). The reason for the low variance percentages is that the images are fundamentally uncorrelated. The variance decreases as control points are added because as features are matched up, the images become less correlated.

Another factor to be considered, in the determination of how many control points to take is the variability in topography across the image. More control points are required in areas of greater slope variability. These areas are characterized by a higher density of ridges and valleys. Feature matching errors in these 'rough' areas are more apparent than in areas of more constant slope.

With the preceding points in mind, the decision to stop taking control points was an iterative one based on three criteria. The first critereon was the change in variance contained in the first principal component. The second critereon was the positional agreement between river and ridgeline features in the vector control data. The final critereon was the absence of 'ghosting' or parallel features appearing in the first principal component image (see figure 20). The first critereon was satisfied with about one-hundred-ten (110) control points in each input image, with variance in the first principal component at fifty-nine percent (59%). The second and third critereon were satisfied at one-hundred-seventy-two (172) points in the ascending input image, and one-hundred-thirty-five (135) in the descending image (figures 15,16). The descending image required fewer control points as it has fewer apparent features.

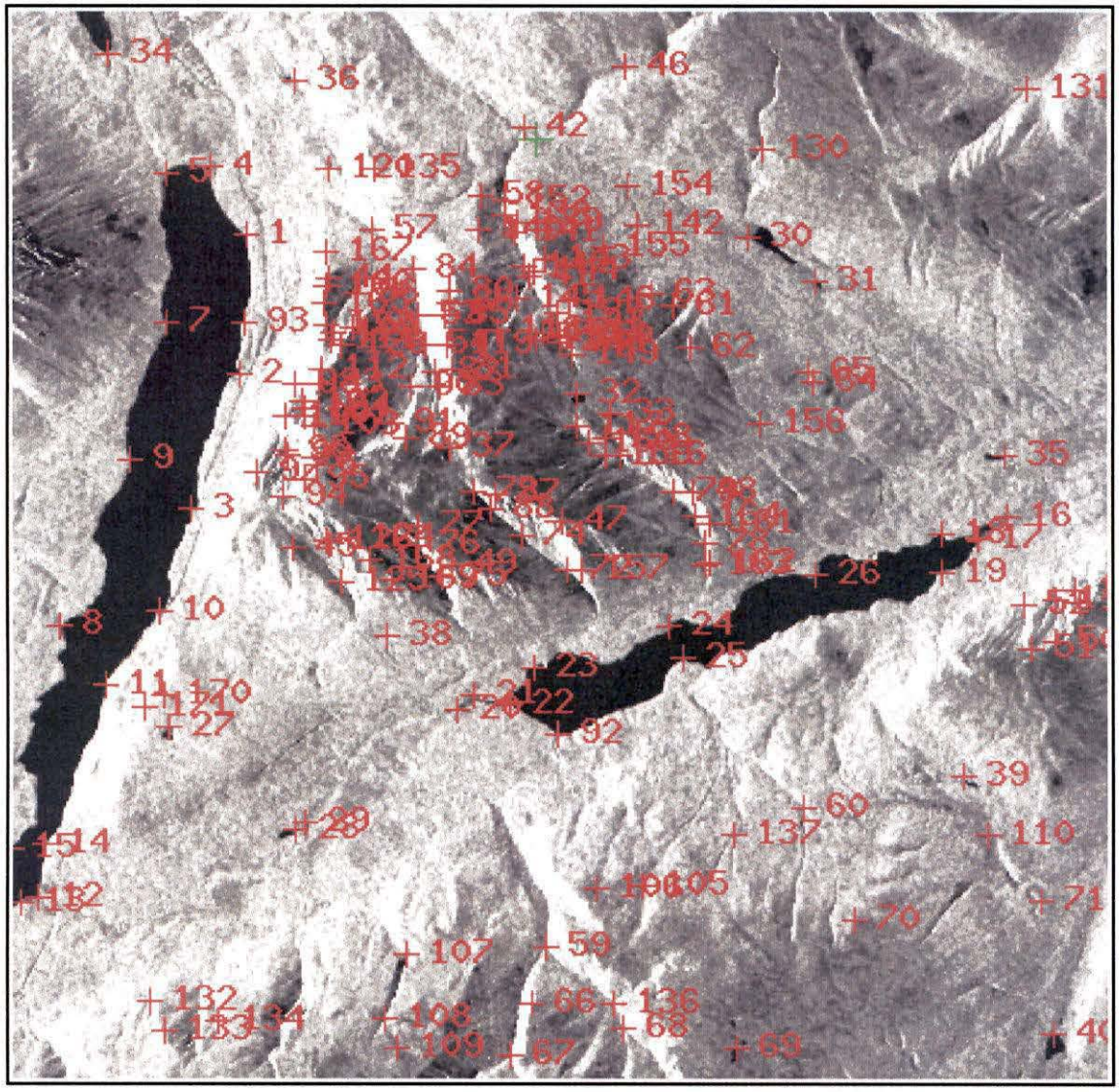

Figure 15. Ascending Geometric Correction Control Points

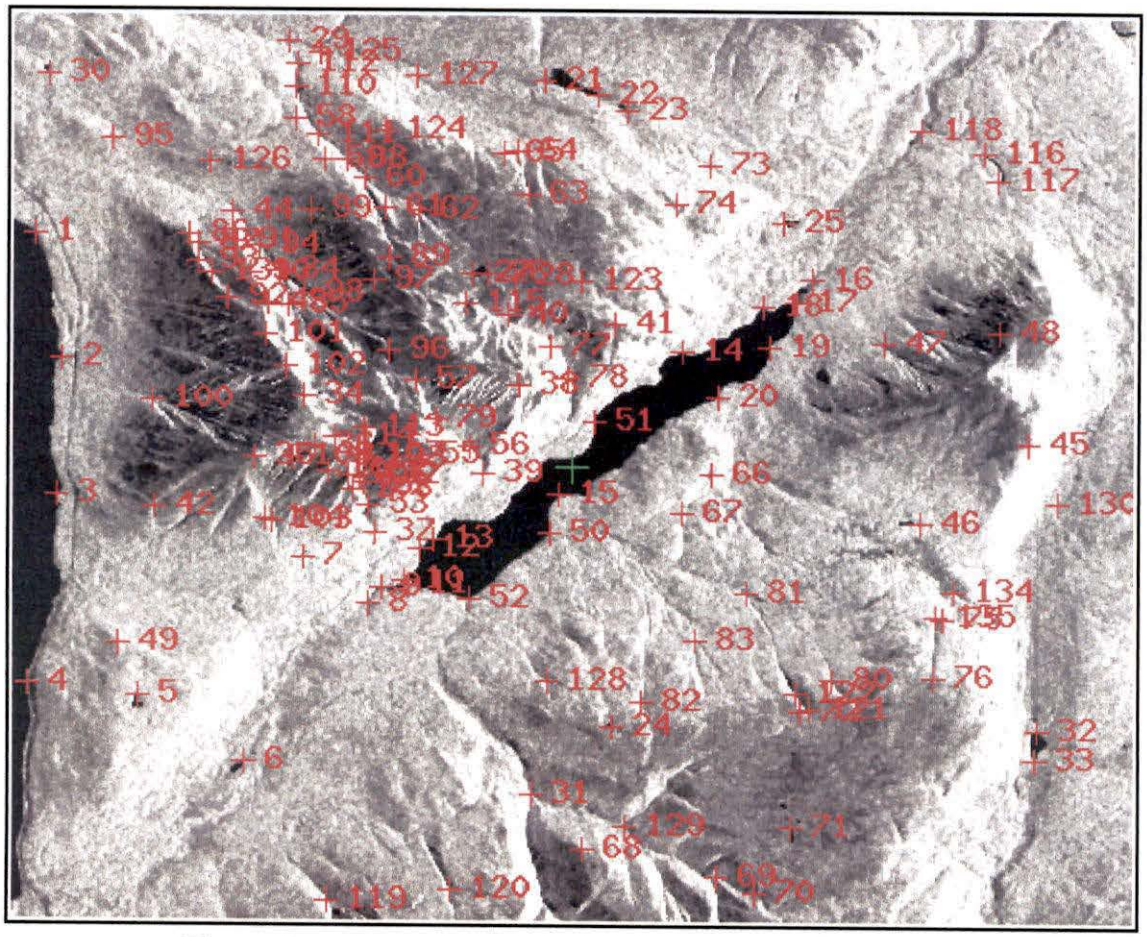

Figure 16. Descending Geometric Correction Control Points

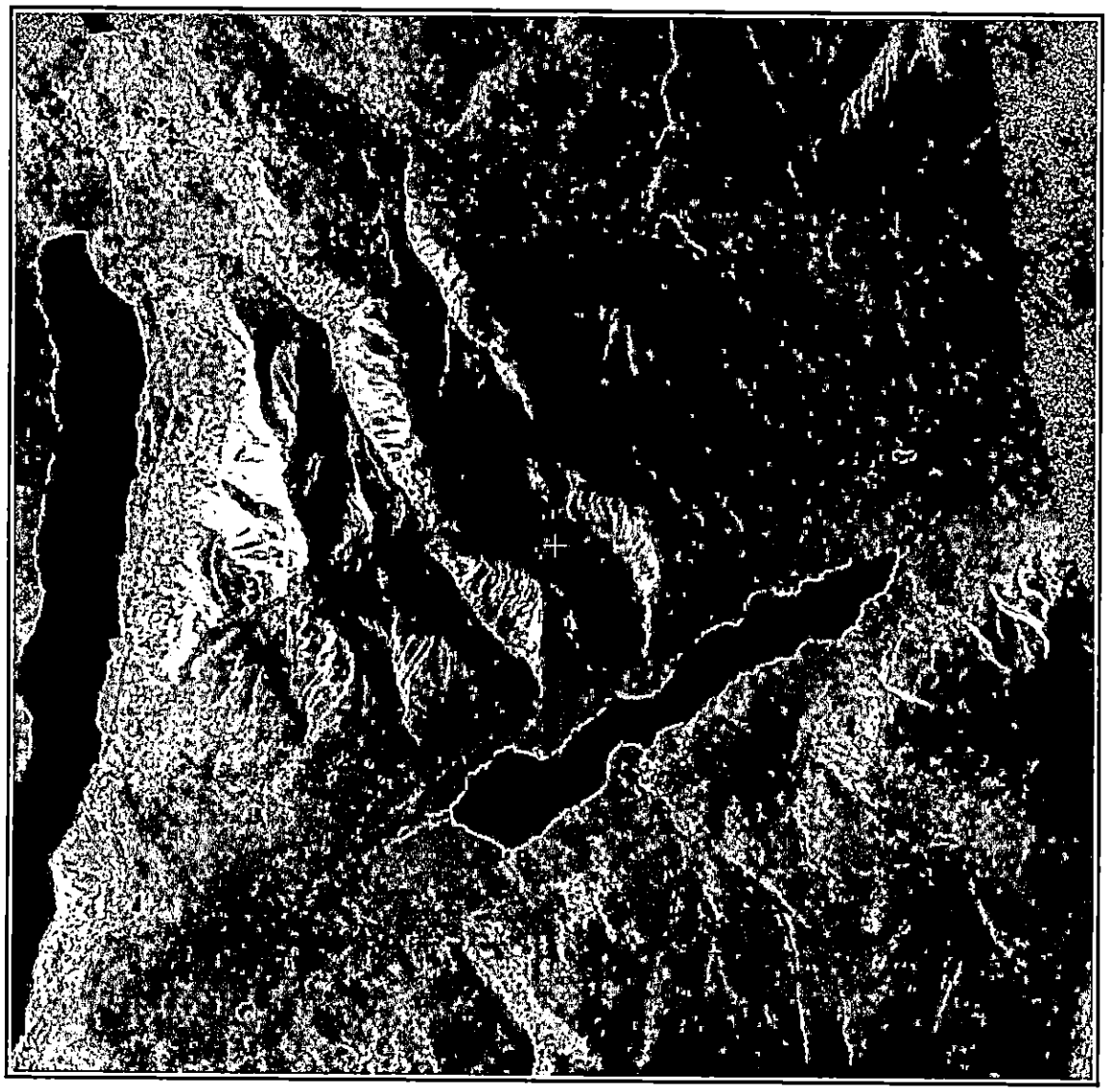

Figure 17. Geometrically Corrected Ascending Imagery

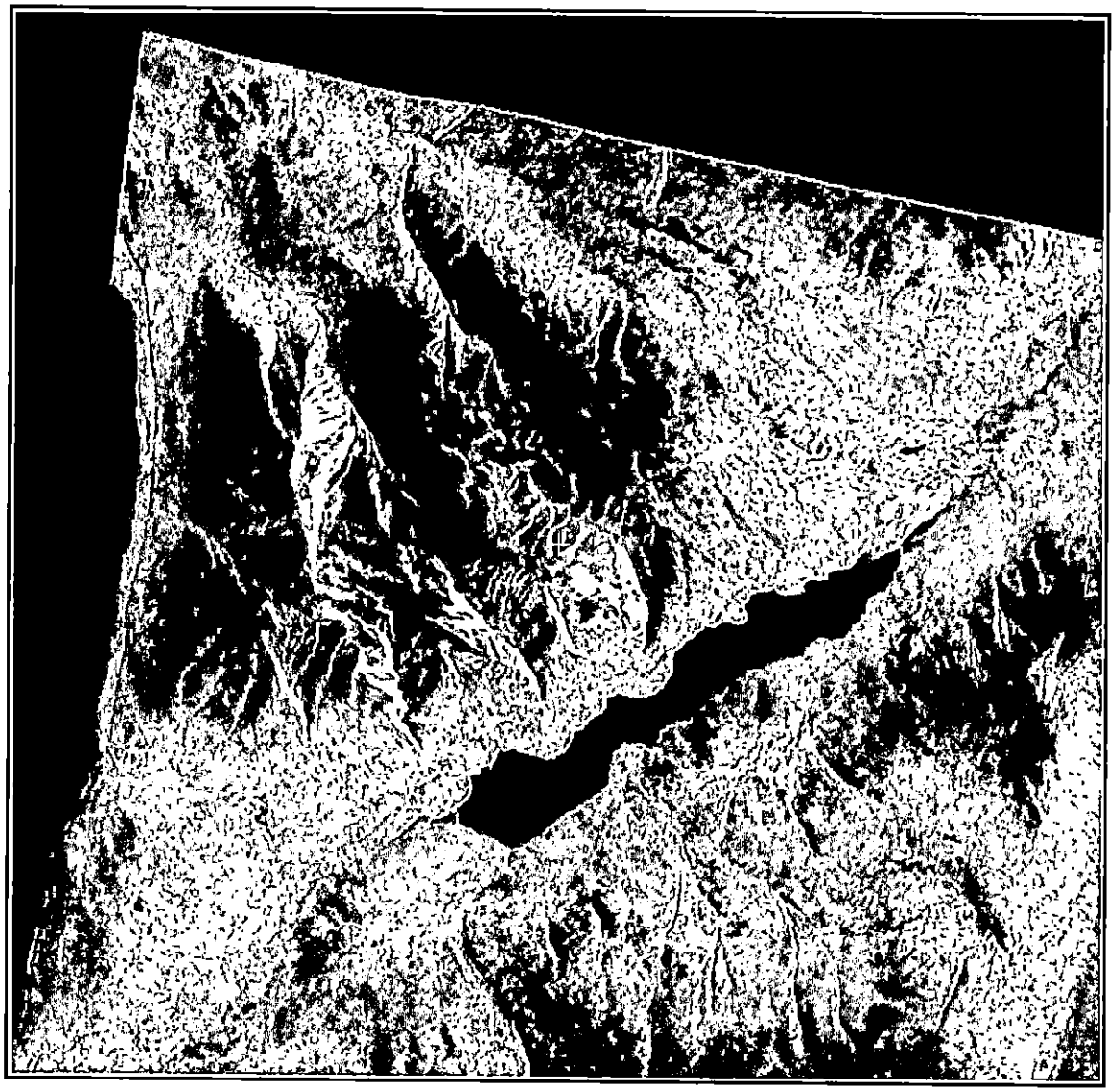

Figure 18. Geometrically Corrected Descending Imagery

5.1.2 Principal Component Analysis

After speckle removal, and geometric correction, the next step in the image data fusion process was the application of principal component analysis. A correlation coefficient of .08 indicates that there is little correlation between the two input images (figure 19). This is reflected in the first principal component containing only fifty-nine percent (59%) of the variance present in both images. As both input images

where produced by the same sensor, looking at the same terrain, it can be assumed that the first principal component of the two images, if completely uncorrelated, would contain fifty (50%) of the variance. Therefore, the first principal component in this case contains eighteen percent more information in the form of variance than either of the input images. A look at the first principal component imagery (figure 20) suggests that most of this extra information was in the textured or 'vegetated' areas, as these regions are much more clearly defined here than in either of the input images.

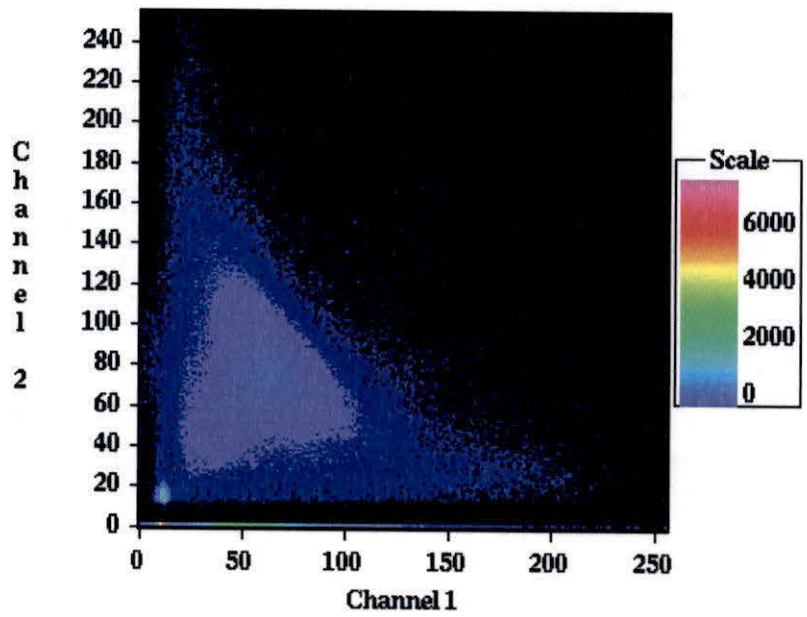

Figure 19. Scatter Plot of Ascending (Channel 1) and Descending (Channel 2) Images

In addition to the apparent enhancement of textured features in the first principal component the principal component analysis also performs the function of selecting as a basis for further data fusion operations the image (ascending or descending) least impacted by foreshortening, layover and shadow. This, since it is conjectured that these effects lessen the variance in the impacted areas and in the image overall.

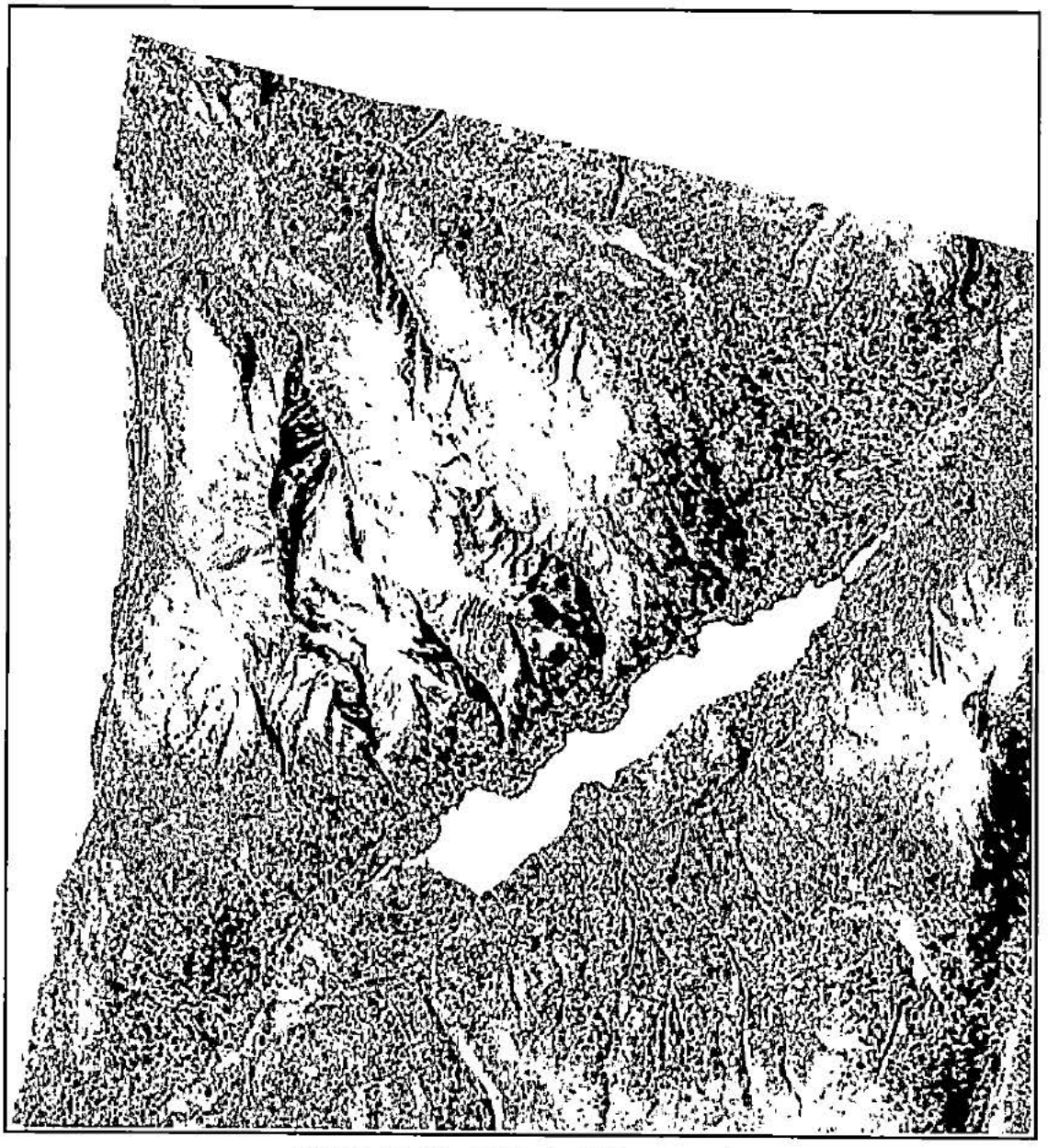

Figure 20. First Principal Component

5.1.3 Application of Facing Slope Mask

A side effect of the principal component analysis is, that while the first

principal component contains the feature set of the the descending imagery, the apparent shadowing suggests it is an ascending image. This is a result of both the uncorrelated nature of the input imagery and the computational restrictions involved when dealing with 16 bit unsigned imagery. In figures 21 and 22 it can be seen that the histograms for the two input images are similar. This is borne out numerically from similar mean values of 11,233.77 for the ascending image, and 9,385.19 for the descending image. The deviations are also similar at .49 and .58 respectively (appendix IV). Since the two images are largely uncorrelated, the axes when transposed during the principal component analysis are not significantly rotated and the first principal component simply corresponds to the histogram of the image with the greatest variance or deviation. In this case, the descending image has the greatest variance. The histogram mirroring evident in figure 23 occurred because the data are unsigned 16 bit numbers and the normal practice of setting the new origin as (0,0) is not possible without negative numbers. Hence the transposed pixel values and associated histograms become mirrored about the software imposed default of 32,767 (PCI, 2000). The visual effect of this histogram mirroring is that the relative intensities of pixels are inverted. Bright, sensor facing pixels appear as darker away facing pixels and the image looks as though it is illuminated from the opposite side.

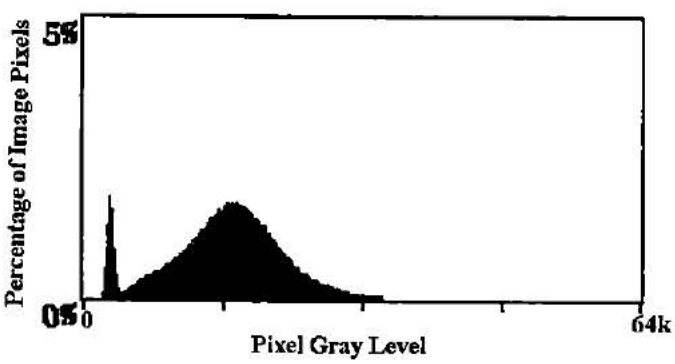

Figure 21. Ascending Image Histogram

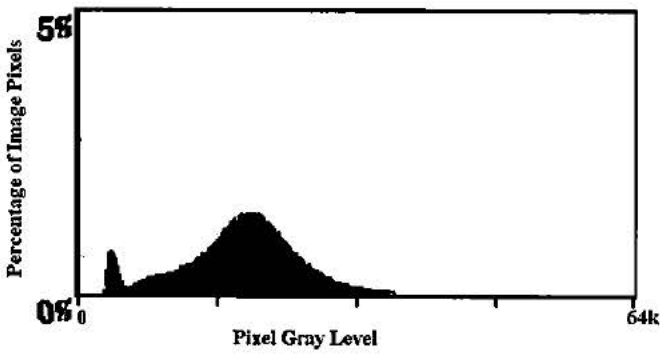

Figure 22. Descending Image Histogram

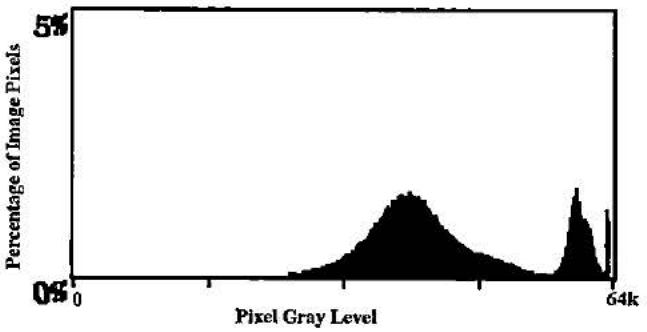

Figure 23. First Principal Component Histogram

Although there has been an apparent increase in textural contrast across the imagery, the number of discernible features (edges) has not changed from the original descending image. Image arithmetic was used to take advantage of the image effects of the principal component analysis and add edge information from the ascending imagery to the first principal component.

A characteristic of facing slopes in SAR imagery is that, given the same surface cover, they are brighter than non-facing slopes. Also, facing slopes are foreshortened, or in the case of steeper slopes, distorted by layover in the imagery. The result of these effects is, that after geometric correction, there is less detail on a facing slope than on other topographies. Since the information to be added to the first principal

component imagery is from facing slopes, consideration was given to avoiding the degradation of detail present on slopes to be enhanced. To this end a mask (figure 24), was created from pixels with values above a certain threshold in the ascending imagery (see appendix II, Image Statistics). This mask corresponds to facing slopes in the ascending imagery, areas that are not well delimited in the descending imagery. Pixels under this mask, in the first principal component imagery, had their values increased by a fixed amount, producing the final output image (figure 25). A fixed value was added to the first principal component under the mask, not the values of the ascending image corresponding to the mask, so as not to degrade the slope detail in the final imagery by adding detail distorted by the effects of foreshortening and layover.

Figure 24. Ascending Facing Slope Mask

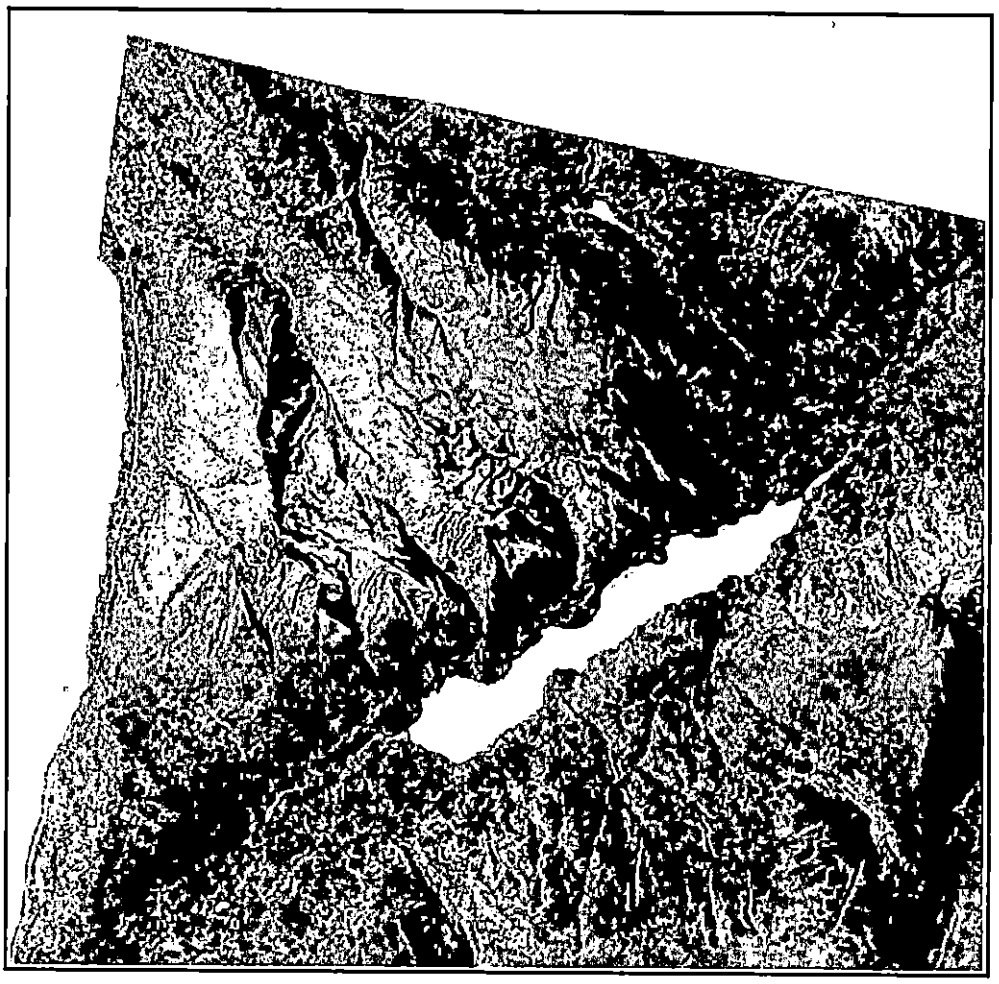

Figure 25. Final Product

5.2 Landform Analysis

From figure 26, the shaded digital elevation model, the basic landforms in the imaged area are clearly delineated. In the centre of the image are four well defined ridgelines running northwest to southeast, bounded on the southeast end by a lake running southwest to northeast, to the west by a lake running north-south and to the east by a large river valley. These ridgelines are divided by three river valleys. To the southeast of the southwest-northeast running lake, is an relatively flat area characterized by a number of smaller river valleys running into the lake from the southeast, bounded by a solitary peak

to the northeast, and river valleys to the far south, and southeast. In the southwest corner of the imageries is a triangular rise separating the lake valleys running north-south and southwest-northeast.

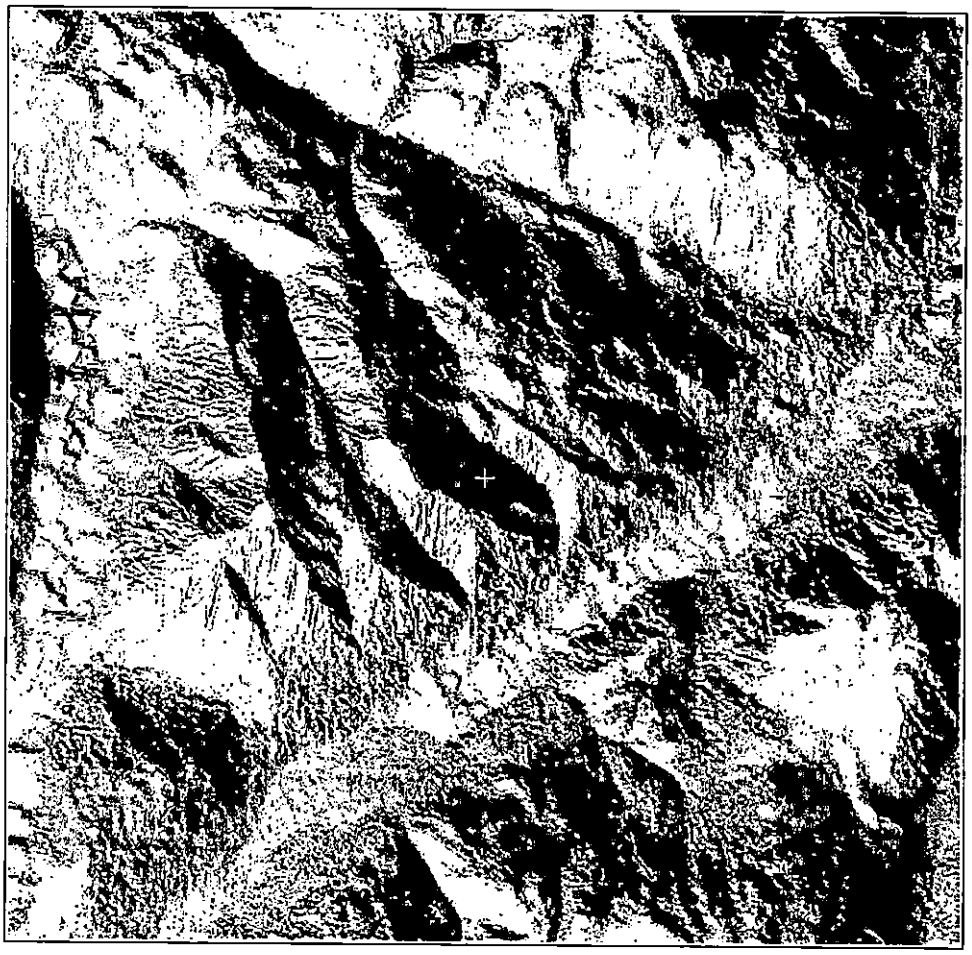

Figure 26. Shadecast on Digital Elevation Model

Both the input images and the output fused image show the basic structure of the landscape. In all three images the major valleys, ridgelines, and lakes are interpretable. Of the two input images the ascending imagery more clearly shows the character of the center ridgelines and valleys. The descending imagery gives a more rounded look to the terrain. As is characteristic of SAR imagery, slope changes on away

facing slopes are hard to detect. An example of this is the valley wall in the extreme southeast corner of the image, which is clearly visible in the descending image but indefinite in the ascending image. Further evidence of the impact that slope aspect has on SAR imagery is the asymmetrical appearance of river valleys in the input imagery. These valleys are, in fact, quite symmetrical.

The effects of foreshortening and layover are most clearly seen in the ascending imagery where the combination of high backscatter and foreshortening has obscured most of the detail on facing slopes. There is a similar loss of detail in the descending image but, because the east facing slopes are in general less steep, the image area impacted is less.

The fused imagery shows improvement over either of the input images, in that it is closer to the shaded relief model in defining terrain topography. Further, the smaller river and valley features are much better defined and appear more symmetric. Features notably more interpretable, are the peak to the east of the central lake, the triangular plateau in the southwest corner and the valley walls in the southeast corner. Much of the facing slope detail, obscured in the ascending imagery, has been replaced by descending image information.

A characteristic of the terrain, evident in the shaded terrain model, and to some extent in the ascending imagery, but missing from the descending and fused imagery, is the sharpness of some of the ridges. In particular, the three ridgelines in the centre of the fused image are rounded when compared to the terrain model.

5.3 Numerical Tests

5.3.1 Texture Classification

Texture classifications were performed on the ascending and descending RADARSAT imageries before speckle removal, on the ascending RADARSAT imagery after speckle removal, and on the final fused product (see appendix III, Process Parameters). The resultant classifications were assessed against Thematic Mapper

imagery classified into four classes: forest, water, barren and rock/beach. In this case, the classified Thematic Mapper imagery is being used as a substitute for ground truth.

Here, it should be noted that there are some fundamental differences between the spatially based texture classifications and the spectrally based Thematic Mapper classifications. First, there are the differences in resolution. The geometrically corrected RADARSAT imagery has a resolution of less than 10 metres while the Thematic Mapper mosaic imagery has a resolution of approximately 50 metres. Second, the sensors are different in how they respond to surface texture. Finally, the texture measure of a pixel based on the values of pixels around it, is different from a spectral classification, based on the neighborhood of a pixel in several spectral bands. As a result of these differences the texture classifications do not form the homogenous regions that are apparent in the unsupervised classification of the Thematic Mapper imagery. Instead the classifications appear to be more on a pixel scale, with indistinct regional boundaries. Although the texture classifications could have been made to present clearer boundaries and perhaps improved the following results by extensive smoothing or the use of polygon growing algorithms, it was decided that the raw classifications would provide more 'honest' results.

The texture classification, of the raw input imageries before speckle removal, produced the results in figures 27 and 28. In both classifications, the effects of viewing angle are clearly evident, the shadowed faces showing little texture information. The confusion matrix (tables 1 and 2) for these classifications show that 93% and 92% of the area classified as forest in the Thematic Mapper imagery was also classified as forest in the RADARSAT imagery. This would seem to be a good result until it is noted that over 50% of the area classified as non-forest in the TM imagery was classified as forest in the RADARSAT imagery. Further, the classification discrepancies detailed in tables 3 and 4 show that, discounting the water classification, more than 60% of the area classified as non-forested in the TM imagery was misclassified by the texture classification.

	# Pixels	*Texture Classified as Forest (#Pixels)*	*Texture Classified as Forest (Percent)*	*Texture Classified as Non-Forest (#Pixels)*	*Texture Classified as Non-Forest (Percent)*
TM Forest	48786	45384	93	3402	7
TM Non-Forest	18190	10262	56	7982	44

Table1. Texture Classification Confusion Matrix (Unfiltered Ascending)

	#Pixels	*Texture Classified as Forest (#Pixels)*	*Texture Classified as Forest (Percent)*	*Texture Classified as Non-Forest (#Pixels)*	*Texture Classified as Non-Forest (Percent)*
TM Forest	48786	45089	92	3697	8
TM Non-Forest	18190	9714	53	8476	47

Table2. Texture Classification Confusion Matrix (Unfiltered Descending)

TM Classified Water Texture Classified as Forest	*TM Classified Barren Texture Classified as Forest*	*TM Classified Rock/Beach Texture Classified as Forest*
4%	67%	64%

Table 3. Classification Conflict Detail (Unfiltered Ascending)

TM Classified Water Texture Classified as Forest	*TM Classified Barren Texture Classified as Forest*	*TM Classified Rock/Beach Texture Classified as Forest*
3%	68%	52%

Table 4. Classification Conflict Detail (Unfiltered Descending)

The texture classifications of the despeckled image (figure 29) produced poor results. This was expected, as the despeckle filter does not differentiate between variance

caused by random noise and variance caused by relatively small objects such as trees. This causes much of the texture information related to the forest cover to be removed in the despeckle process. This is a well known problem and is noted in the software documentation (PCI, 2000). That the texture classification of despeckled imagery is inappropriate is demonstrated in table 5 which shows that only 2% of the area classified as forest in the TM imagery was also classified as forest in the despeckled RADARSAT imagery. Here, the errors of omission are large, where in the case of the 'raw' imagery, the errors were mostly of commission. Errors of omission occur when areas of a type are excluded from the classification. Errors of commission occur when areas not of a type are included in the classification.

	#Pixels	*Texture Classified as Forest (#Pixels)*	*Texture Classified as Forest (Percent)*	*Texture Classified as Non-Forest (#Pixels)*	*Texture Classified as Non-Forest (Percent)*
TM Forest	48786	856	2	47930	98
TM Non-Forest	18190	1027	6	17163	94

Table 5. Texture Classification Confusion Matrix (Despeckled Ascending)

TM Classified Water Texture Classified as Forest	*TM Classified Barren Texture Classified as Forest*	*TM Classified Rock/Beach Texture Classified as Forest*
1%	6%	9%

Table 6. Classification Conflict Detail (Despeckled Ascending)

The texture classification of the fused imagery, using the same inputs as used in the previous classifications, produced the results presented in figure 30 and detailed in tables 7 and 8. Comparing these results; with the classifications of the unfiltered and

despeckled imageries, the most notable difference is that there is a better balance between errors of omission and commission. Table 7 shows that 56% of the area, classified by texture to be forest in the fused imagery, was actually forest according to the classified TM imagery. Conversely, it shows that 32% of the land, classified as being forest in the fused imagery, was not. The most poorly classified cover is 'Rock/Beach', with 45% percent classified as forest (table 8). The best result was the water classification, where only 6% was misclassified as forest. Finally, contributing to a better overall classification, the classification of an area as forest in the fused imagery was not dependent upon whether it was on a facing slope, as it was in the unfiltered input imagery.

	#Pixels	***Texture Classified as Forest (#Pixels)***	***Texture Classified as Forest (Percent)***	***Texture Classified as Non-Forest (#Pixels)***	***Texture Classified as Non-Forest (Percent)***
TM Forest	48786	27211	56	21575	44
TM Non-Forest	18190	5899	32	12291	68

Table 7. Texture Classification Confusion Matrix (Fused Imagery)

TM Classified Water Texture Classified as Forest	***TM Classified Barren Texture Classified as Forest***	***TM Classified Rock/Beach Texture Classified as Forest***
6%	35%	45%

Table 8. Classification Conflict Detail (Fused Imagery)

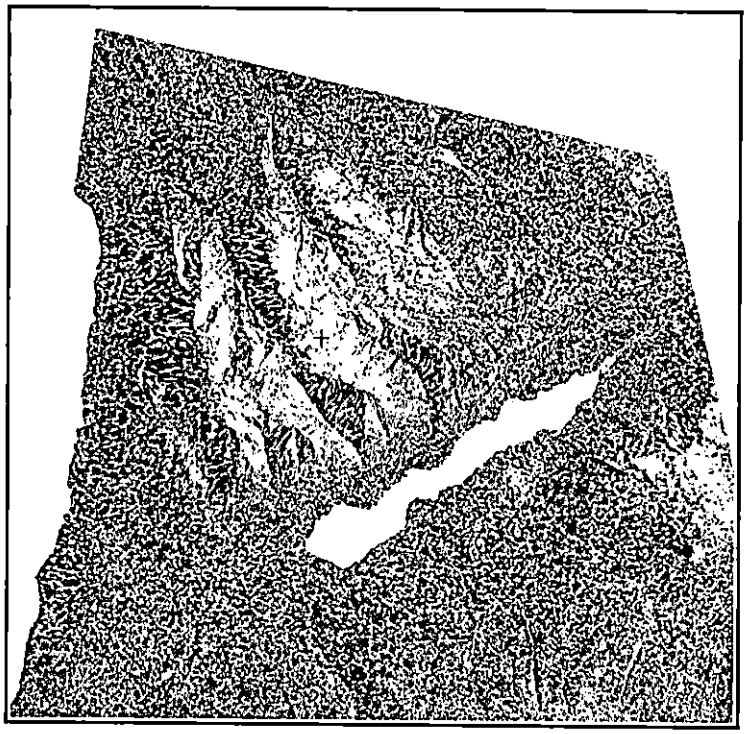

Figure 27. Texture Classification of Unfiltered Ascending Image

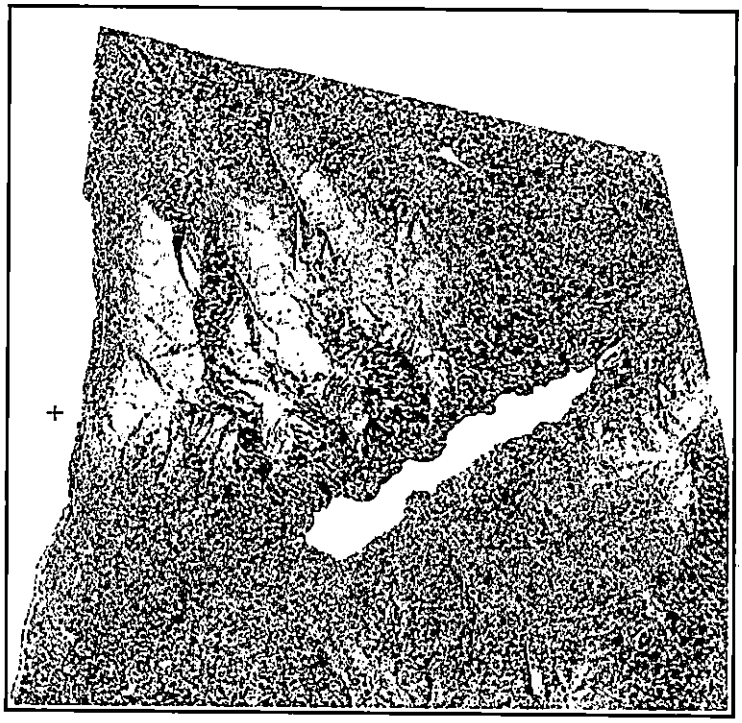

Figure 28. Texture Classification of Unfiltered Descending Image

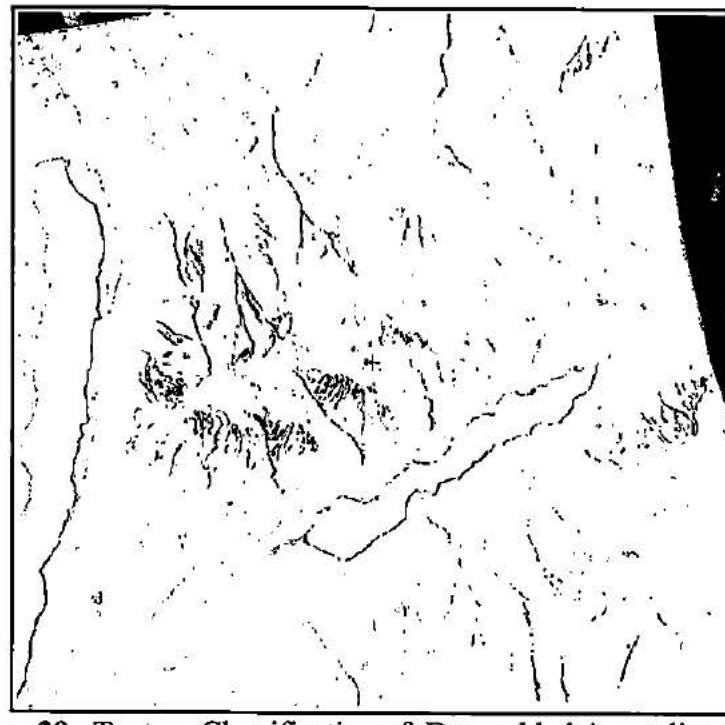

Figure 29. Texture Classification of Despeckled Ascending Image

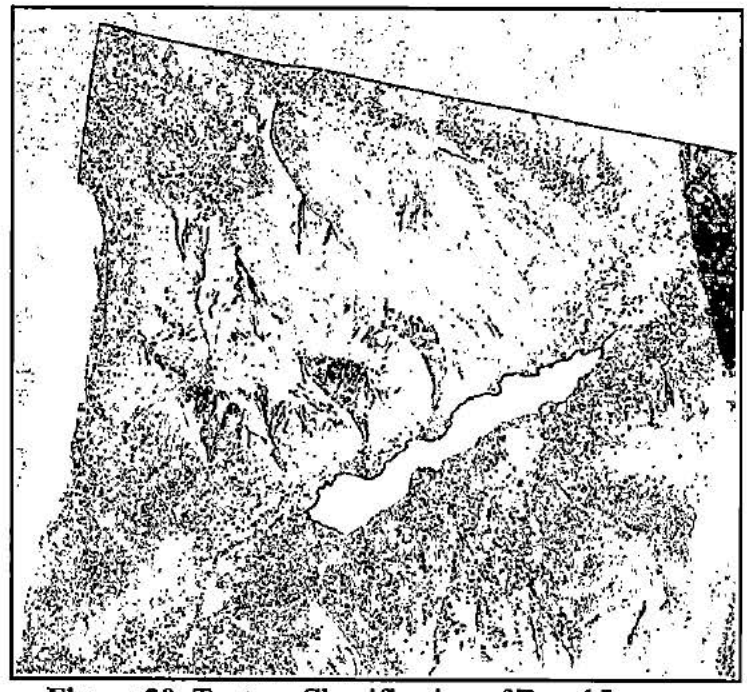

Figure 30. Texture Classification of Fused Imagery

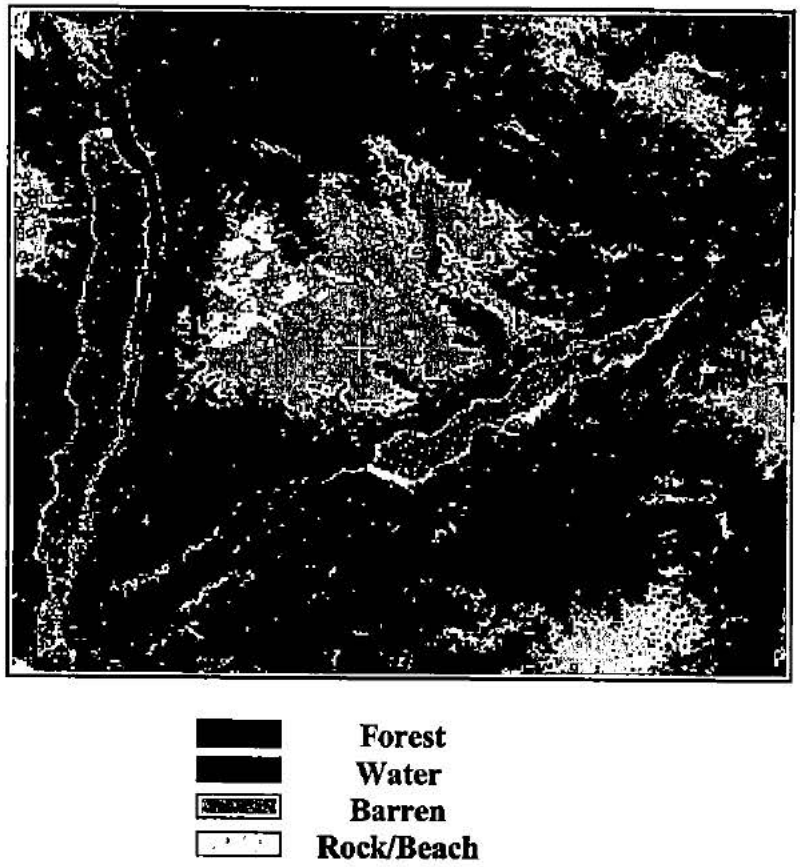

Figure 31. Classified Thematic Mapper Imagery

5.3.2 Lineament Detection

Lineaments in SAR imagery, and in remotely sensed imagery in general, are the boundaries between regions of homogeneous image intensity. In this project the presence or absence of certain lineaments is used as a measure of the success of the fusion process. Ideally, all lineaments present in either input image are also present in the fused imagery. Unlike the case of texture classification, automatic lineament detection can only be successfully performed on despeckled imagery. Here, the lineaments were determined using the LINE function in the PCI software using the same parameters on the two

despeckled input images and the fused image (see appendix III,Computer Processing Parameters).

The LINE function attempts to do, by numerical methods, what is easily done by the human visual system (PCI, 2000). Whereas the human visual system can easily associate a number of segments of varying intensity and orientation into one contiguous lineament, this association requires complicated algorithms and the consideration of a significant number of parameters in the numerical model. The number and nature of lineaments detected by the LINE function vary widely depending upon both the input parameters to the function and enhancements made to the imagery. Attempts to tune the input parameters to detect what are, to the eye, significant lineaments may result in the generation of large numbers of spurious lineaments. Similarly, changes to the fusion process to ease the automatic detection of lineaments may create an image that is otherwise less interpretable.

The numerical determination of lineaments is also complicated by problems in accuracy assessment. Unless there is perfect geometric agreement between the detected lineaments and digital ground truth data, a numeric accuracy assessment is unreliable. A thorough manually assisted accuracy assessment in the absence of geometrically compatible digital data, is impractical except for small areas or areas with few lineaments. Another problem associated with error assessment is the lack of differentiation in the numerical solution between different types of lineaments. The available lineament detection programs do not and cannot, without ancillary data, differentiate water course lineaments from ridge lineaments or valley bottom lineaments from vegetation boundary lineaments. These problems in lineament detection, and accuracy assessment, mean that all that can be said with certainty, based on the numerical model, is the number and length of lineaments detected by a certain set of parameters. Whether certain kinds of lineaments are favoured in different images, or that particular lineaments are present in all three images, can only be determined with the aid of a visual assessment.

Here, the parameters in the automatic lineament detection program (LINE) were selected such that the density of lineaments generated was similar to the density of river and ridge features provided in the TRIM vector data. The lineaments detected using these parameters show clear differences between the three result sets. While all three sets contain lineaments defining the major ridgelines and rivers, the line features representing slope breaks and slope detail vary between sets. In most cases lineaments found in either the ascending or descending images are present in the fused imagery. An exception is the region shown in the circled areas in figures 32 through 34. Here, ridgeline and slope detail lineaments, that are clearly visible in the ascending image and absent in the descending image, are present but not well defined in the fused imagery. This illustrates the problem that prompted the application of the facing slope mask. However, increasing the image values under the mask to levels which would allow the lineament detection algorithm to detect these specific linear features, degrades the image elsewhere, particularly in terms of surface detail in areas of high backscatter intensity.

The numerical support for the contention that there is a merging of linear features from the two input images is outlined in table 9. As discussed previously, an absolutely objective assessment of lineament detection accuracy is not possible. However, the statistics indicate that more lineaments are detectable using the LINE function in the fused imagery than in either the ascending or descending image. This supports the subjective opinion that there has been a 'merging' of features through the fusion process.

	Ascending	***Descending***	***Fused***
Number of Lineaments	2591	2710	2854
Total length of Lineaments (Kilometers)	768	797	805

Table 9. Detected Lineaments

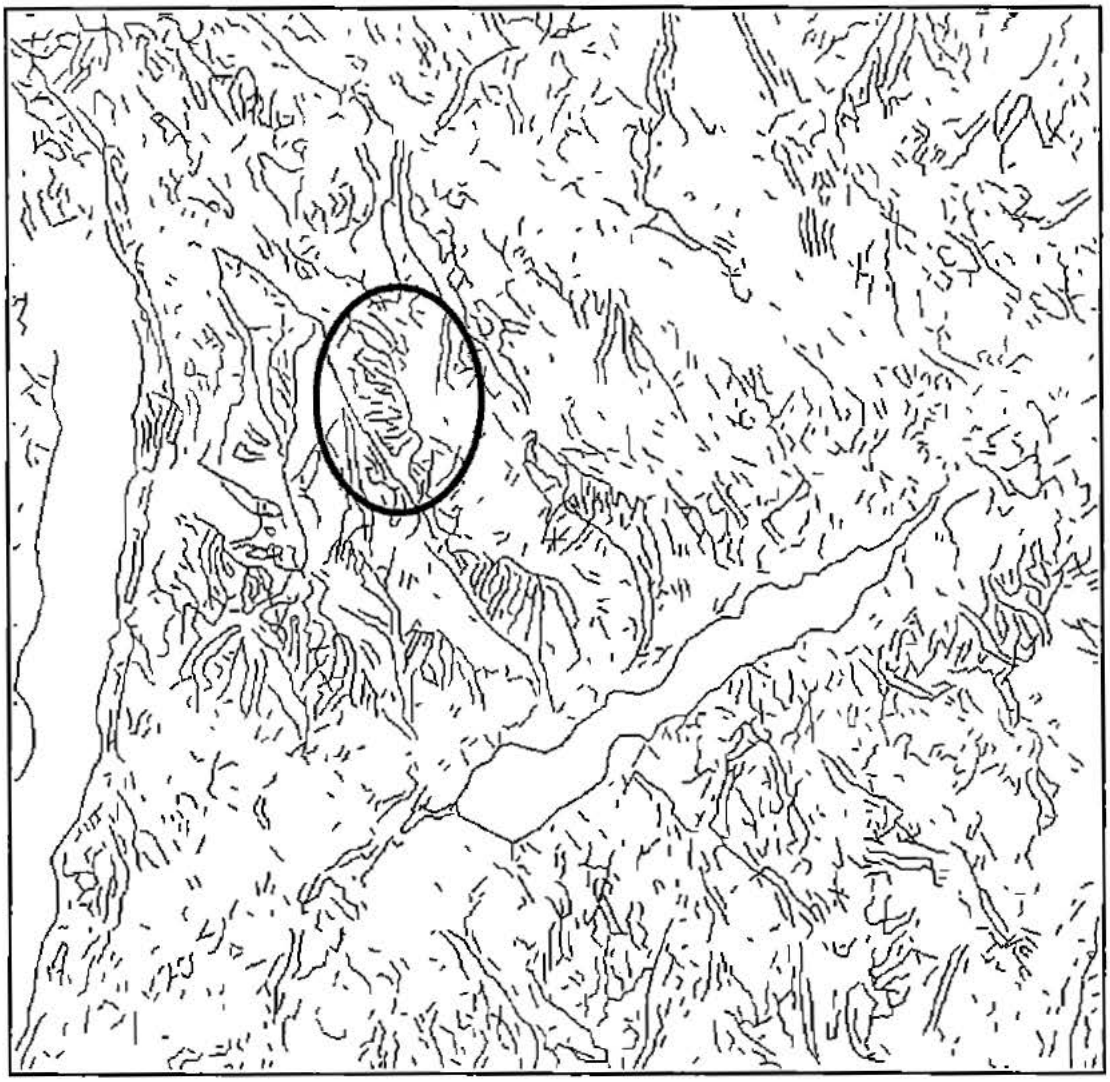

Figure 32. Ascending Image Lineaments

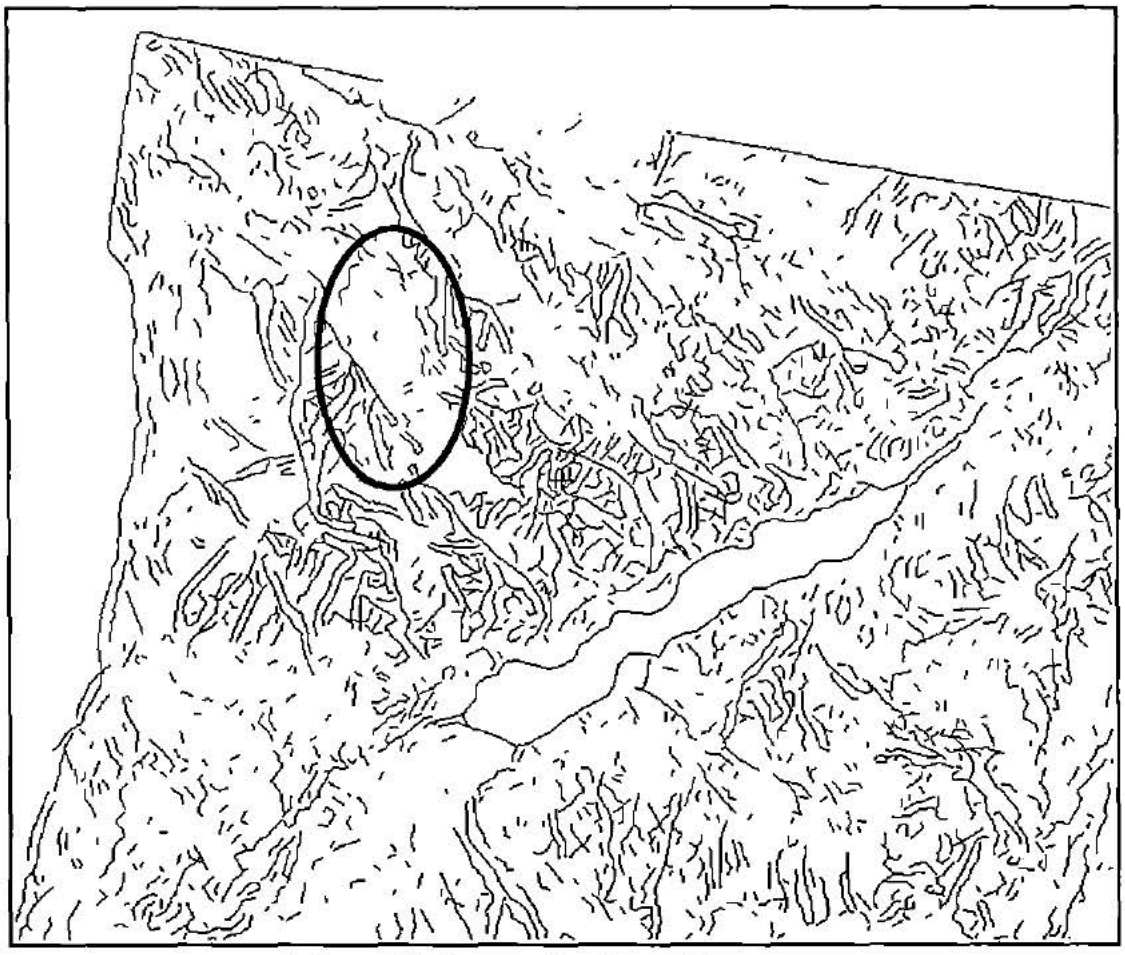

Figure 33. Descending Image Lineaments

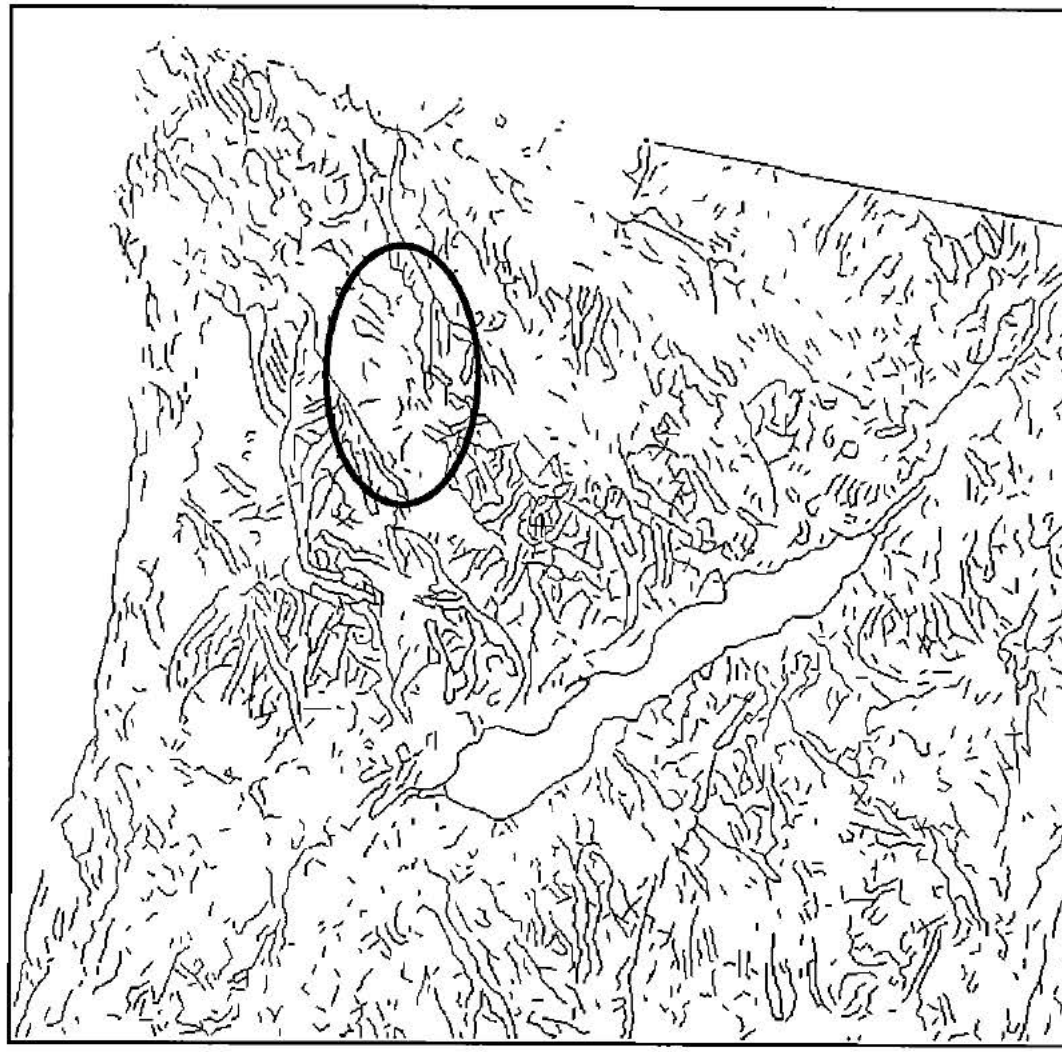

Figure 34. Fused Image Lineaments

Chapter 6

Conclusions

6.0 Introduction

This chapter discusses the conclusions drawn from this project and possible areas of future study. It begins with a summary of the fusion process and an assessment of the overall success of the project with respect to its goals. Secondly, it discusses the key points that either contributed to, or impeded, that success. In discussing the key points of the project, opportunities for future research are identified. These research opportunities can be the search for solutions to problems encountered in the study or the application of the methodology to other data environments.

6.1 Project Summary

The major steps in the fusion of the ascending and descending RADARSAT images of high relief terrain, along with related concerns and results are:

1) The imagery was despeckled to aid in the selection of control points for geometric correction and to simplify image interpretation.
2) Image matching was performed on the imagery to allow for the merging of the opposing look images. The images were geometrically corrected to river and ridge data to permit comparison to other data types. The collection of control points was adversely affected by the effects terrain relief had on the RADARSAT imagery, particularly the effects of foreshortening, layover and shadowing.
3) Principal component analysis was performed on the despeckled, image matched, ascending and descending

image pair. This produced an image, the first principal component, that possessed three properties. One, it showed more pronounced differences in terrain cover, apparent through changes in texture, than the input images. Two, the image was, in terms of feature content, the descending image, the image with the greatest variance and conjectured to be least affected by foreshortening, layover and shadow. Finally, the image was inverted with regards to pixel grey scale intensity because of the characteristics of unsigned 16 bit arithmetic.

4) An image mask was generated from the ascending look imagery (conjectured to be most affected by foreshortening etc.) which covered the sensor facing slopes. Values of pixels under this mask in the first principal component imagery were raised by a fixed amount to provide visual relief, enhance slope breaks and not alter the grey level relationships between pixels under the mask. If real arithmetic was used in the principal component analysis and the grey levels not inverted, then the pixel values under the mask would have been decreased to achieve similar results.

6.2 Overall Assessment

The primary goal of this project was to increase the utility of RADARSAT imagery through the combination, or fusion, of an ascending and descending pair. The imagery covered an area of high relief with the accompanying issues of geometry hindering classification.

The most significant improvement, both in terms of effort required to arrive at the

enhancement and in end user utility, was the increased differentiation of texture across the image. Both in terms of subjective image quality and amenability to the automated determination of texture classes, the final product was superior to either of the input images.

There was less success with the combination of lineament elements in the ascending/descending pair. First, more processing was required in acquiring control points, generating the slope masks and performing the arithmetic operation. Second, although it was successful from a subjective standpoint in that the various ridge and valley features were more identifiable in the final imagery than in the input imagery, it was only partially successful from a automated detection standpoint. Here, it became a question of how much degradation in the visual quality of the output image was acceptable to allow for a better computed classification. To make it possible for the digital algorithms to detect all lineaments present in the input images, it would have been necessary to increase the slope contrast to the point where textural classification and overall image interpretation would suffer.

6.3 Project Key Points

The provision that the data fusion take place without the aid of a digital terrain model was the most important constraint on the project. It restricted the methodology used to geometrically correct the input imagery to a process dependent upon operator input. The number of control points identifiable by an operator in both the input imagery and vector data is limited, restricting the possible fusion techniques to those less sensitive to image matching precision. Although there has been some work on the automated geometric correction of SAR imagery (Gelautz *et al.*, 1997) these works require a digital terrain model. Since, if we remain within the constraints of this project, a digital terrain model is not available, other approaches need to be explored. Since the matching of the RADARSAT imagery was the most time consuming and hence, most costly aspect of this project; research into improvements to the geometric correction process will be the most

beneficial to the methodology as a whole.

The decision to use imagery from an area of high relief was made because both the problems and the impact of solutions to those problems, is more easily seen in this imagery than in imagery of flatter terrain. Using imagery from an area of high relief to develop the fusion process had advantages and disadvantages. Matching the input imagery was more difficult, because the roughness of the terrain resulted in many localized distortions each requiring its own set of control points to correct. Counter to this, the terrain provided a large number of distinct edge features, ridges, valleys, rivers etc., that could be used to identify the needed control points. In flatter, more rolling terrain slope transitions are harder to determine and ridge and valley features are less distinct, making the collection of control points more difficult. However, in flatter terrain fewer control points would be needed. An avenue for further study would be to apply this fusion method to a variety of terrain topographies, from rough to smooth, to determine where the greatest improvements are attained in terms of costs and benefits.

This project chose as its study site an area where the major linear features run roughly parallel to the flight path of the satellite. This was done because edges running parallel to the sensor path show more distinctly than features that are at right angles to the flight path. It is easier to find control points on parallel features and to quantify the enhancement of those features. A further step in the study might be the application of the fusion technique developed here to areas where the features do not run parallel to the sensor to see if similar improvements in imagery are attained.

6.4 Generalization of Methodology to other Data Environments

The adaptation of the methodology developed here to other opposing image data sets is impacted by seven factors if using single band SAR imagery:

1) The relief of the area to be fused.
2) The complexity of the area topology.

3) Size of the area covered by the imagery.
4) Pixel resolution of the imagery.
5) Data type of the imagery.
6) The imaging geometry of the two opposing looks.
7) Orientation of terrain features.

The relief of the area to be fused, as discussed previously in this chapter, impacts both the difficulty in performing the fusion and the utility of that fusion. The greater the relief, the greater the problems in geometric correction, but the more useful the result. In areas of low relief the result would not be significantly different from the input images.

The complexity of the topography impacts the difficulty in geometrically correcting the input imagery. For a given relief, more features require more control points. The two other factors that impact the geometric correction of imagery are the size of the area imaged, and the pixel resolution of the imagery. These factors, in combination, dictate the amount of data to be processed which, in turn, affects the cost of processing. These factors also govern the cost of processing in all other steps of the methodology.

It may be that it is not always true that the image least impacted by foreshortening, layover and shadow will have the greatest variance and hence dominate the first principal component. If it is not true, then the determination of which imagery provides the slope mask is less automatic and the image fusion will probably be less successful. In any case, more study areas need to be considered to determine if the assertion that, the first principal component is dominated by information from the imagery least affected by terrain geometry considerations, is true.

In considering the imaging geometry of the opposing looks, both the relationship with the sensor to ground and the relationship between the look angles have to be taken into account. The nearer the sensor is to nadir, the less foreshortening, shadowing, and layover affect the imagery and the less need there is for fusing the imagery. Also different

results can be expected as the angle on the ground between the two looks decreases from 180°.

The final consideration is the orientation of terrain features with respect to the sensors. As mentioned previously, linear features running parallel to the flight path of the sensor are more easily detected that ones running perpendicular to the sensor. Thus, better results can be expected for example, in the case of RADARSAT data, in fusing imagery whose features run mostly north-south.

References

Ahern, F.J., I. McKirdy, and J. Brown, 1996, Boreal Forest Information Content of Multi-Season, Multi-Polarization C-Band SAR Data, *Canadian Journal of Remote Sensing*, 22(4):456-472.

Alaska SAR Facility, 1995, SAR Processing Site, http://www.asf.alaska.edu/ .

Brown, R.J., B. Brisco, M.A. D'Iorio, C. Provost, R.A. Ryerson, and V. Singroy, 1996, RADARSAT Applications: Review of GlobeSAR Program, *Canadian Journal of Remote Sensing*, 22(4):404-419.

Chavez, P.S., Jr., S.C. Sides, and J.A. Anderson, 1991, Comparison of Three Different Methods to Merge Multiresolution and Multispectral Data: Landsat TM and SPOT Panchromatic, *Photogrammetric Engineering and Remote Sensing*, 62(3):295-303.

De Grandi, G.F., M. Leysen, J.S. Lee, and D.Schuler, 1997, Radar Reflectivity Estimation Using Multiple SAR Scenes of the Same Target: Techniques and Applications, *International Geoscience and Remote Sensing Symposium Conference Proceedings.* Compact Disk.

De Moraes Novo, E.M.L., M.P. de F. Costa, and J.E. Mantovani, 1998, RADARSAT Exploratory Survey on Macrophyte Biophysical Parameters in Tropical Reservoirs, *Canadian Journal of Remote Sensing*, 24(4):367-375.

Dobson, C.M., Pierce, L., Kellndorfer, J. and Ulaby F., 1997, Use of SAR Image Texture in Terrain Classification, *International Geoscience and Remote Sensing Symposium Conference Proceedings.* Compact Disk.

Franklin, S.E., and C.F. Blodgett, 1992, An Example of Satellite Multisensor Data Fusion, *Computers and Geosciences*, 19(4):577-583.

Garguet-Duport, B., J. Girel, J. Chassery, and G. Pautou, 1996, The Use of Multiresolution Analysis and Wavelets Transform for Merging SPOT Panchromatic and Multispectral Image Data, *Photogrammetric Engineering and Remote Sensing*, 62(9):1057-1066.

Gelautz, M., E. Mitteregger, and F. Leberl, 1997, Automated Acquisition of Ground Control Using SAR Layover and Shadows, *International Geoscience and Remote Sensing Symposium Conference Proceedings.* Compact Disk.

Grunsky, E., 1995, An Evaluation of RADARSAT For Mult-Disiplinary Geological Mapping in British Columbia, *Proposal to Canadian Space Agency, ADRO Project.*

Heikkonen, J., I. Kanellopoulos, A. Varfis, A. Steel. and K. Fullerton, 1997, Urban Land Use Mapping with Multi-Spectral and SAR Satellite Data Using Neural Networks, *International Geoscience and Remote Sensing Symposium Conference Proceedings.* Compact Disk.

Jensen, J.R., 1986, *Introductory Digital Image Processing*, New Jersey, Simon and Schuster.

Karnieli, A., A. Meisels, L. Fisher, and Y. Arkin, 1996, Automatic Extraction and Evaluation of Geological Linear Features from Digital Remote Sensing Data Using a Hough Transform, *Photogrammetric Engineering and Remote Sensing,* 62(5):525-531.

Kux, H.J.H., J.R. dos Santos, F.J. Ahern, R.W. Pietsch, and M.S.P. Lacruz, 1998, Evaluation of RADARSAT for Land Use and Land Cover Dynamics in the Southwestern Brazilian Amazon State of Acre, *Canadian Journal of Remote Sensing,* 42(4):350-359.

Lillesand, T., and R. Kiefer, 1987, Remote Sensing and Image Interpretation, 2nd edition, John Wiley and Sons, New York.

Marinelli, L., O. Ferger, L. Laurore, and V. Poujade, 1997, Relief Restitution by Radargrammetry Using RADARSAT Images, *International Geoscience and Remote Sensing Symposium Conference Proceedings.* Compact Disk.

Pairman D. and S. McNeill, 1997, Efficient Calculation in the Map Domain of SAR Layover and Shadow Masks, *International Geoscience and Remote Sensing Symposium Conference Proceedings.* Compact Disk.

PCI Geomatics, 2000, Using PCI Software Volume 1, Version 6.3, PCI Geomatics, Ontario, Canada.

Pellemans, A.H.J.M., R.W.L. Jordans, and R. Allewijn, 1993, Merging Multispectral and Panchromatic SPOT Images with Respect ot the Radiometric Properties of the Sensor, *Photogrammetric Engineering and Remote Sensing,* 59(1):81-87.

Radarsat International, 1998, Radarsat Interactive, http://www.rsi.ca

Rowan, L.C., and T.L. Bowers, 1995, Analysis of Linear Features Mapped in Landsat Thematic Mapper and Side-Looking Airborne Radar Images of the Reno 1° by 2° Quadrangle, Nevada and California: Implications for Mineral Resource Studies. *Photogrammetric Engineering and Remote Sensing,* 61(6):749-759.

Saether, B., H. Rueslatten, and A. Gronlie, 1994, Application of the Hough Transform for Automated Interpretation of Linear Features in Imageries, *International Geoscience and Remote Sensing Symposium Conference Proceedings.* Compact Disk.

Saint-Jean, R., V. Singhroy, and S.M. Khalifa, 1995, Geological Interpretation of Integrated SAR Images in the Azraq Area of Jordan, *Canadian Journal of Remote Sensing,* 21(4):511-517.

Shimabukuro, Y.E., S.Amaral, F.J. Ahern, and R.W. Pietsch, 1998, Land Cover Classification from RADARSAT Data of the Tapajos National Forest, Brazil, *Canadian Journal of Remote Sensing*, 24(4):393-401.

Singhroy, V., 1997, Effects of Terrain Types on the Selection of RADARSAT Beam Modes for Geological Mapping, *International Geoscience and Remote Sensing Symposium Conference Proceedings.* Compact Disk.

Sveinsson, J.R., J. Benediktsson, 1997, Tree Structured Filter Banks for Speckle Reduction of SAR Images, *International Geoscience and Remote Sensing Symposium Conference Proceedings.* Compact Disk.

Toutin, T., Y. Carbonneau, and L. St-Laurent, 1992, An Integrated Method to Rectify Airborne Radar Imagery Using DEM, *Photogrammetric Engineering and Remote Sensing,* 58(4):417-422.

Vrabel, J., 1996, Multispectral Imagery Band Sharpening Study, *Photogrammetric Engineering and Remote Sensing,* 62(9):1075-1083.

Wilson, B.A, 1996, Estimating Coniferous Forest Structure using SAR Texture and Tone, *Canadian Journal of Remote Sensing*, 22(4):382-389.

Wivell, C., C. Olmsted, D. Steinwand, and C, Taylor, 1993, Spaceborne Synthetic Aperture Radar Image Intensity Corrections by Composition of Opposing Looks, *Proceedings of the Ninth Thematic Conference on Geologic Remote Sensing,* Environmental Research Institute of Michigan, Ann Arbor, MI.

Yocky, D., 1995, Image Merging and Data Fusion by Means of the Descrete Two-Dimensional Wavelet Transformation, *Journal of the Optical Society of America,* 12(9):1834-1841.

Yocky, D., 1996, MultiresolutionWavelet Decomposition Image Merger of Landsat Thematic Mapper and SPOT Panchromatic Data, *Photogrammetric Engineering and Remote Sensing,* 62(9):1067-1074.

Zwillinger, D. editor, 1995, CRC Standard Mathmatical Tables and Formulas, 30th Edition, CRC Press.

APPENDIX I

RADARSAT Scene Specifications

Ascending Imagery

FILE_TYPE = IMAGE
IMAGE_POINTER = SCENE01\DAT_01.001
SCENE_ID = C0003343
LABEL_RECORDS = 1
LABEL_RECORD_BYTES = 16252
LINE_PREFIX_BYTES = 192
GROUP _SAMPLES = 1
BAND_TYPE = BSQ
IMAGE_BANDS = 1
SAMPLE_BITS = 16
SAMPLE_BITS_USED = 16
SAMPLE_TYPE = UNSIGNED_INTEGER
BYTE_ORDER = MSB
SEMI_MAJOR_AXIS = 6378.140
SEMI_MINOR_AXIS = 6356.755
PLATFORM = RADARSAT_1
IMAGE_RECORD_BYTES = 16144
IMAGE_LINES = 8404
LINE_SAMPLES = 7976
SCENE_ORIENTATION = 351.3266296
SCENE_CENTRE_LAT = 57.777177 (57ø46'37.84")
SCENE_CENTER_LON = -130.17597 (-130ø10'32.87")
UL_CORNER_LAT = 57.975728 (57ø58'32.62")
UL_CORNER_LON = -130.659789 (-130ø39'35.24")
UR_CORNER_LAT = 58.043314 (58ø2'35.93")
UR_CORNER_LON = -129.826314 (-129ø39'34.73")
LL_CORNER_LAT = 57.509656 (57ø30'34.76")
LL_CORNER_LON = -130.519461 (-130ø31'10.06")
LR_CORNER_LAT = 57.577168 (57ø34'37.80")
LR_CORNER_LON = -129.696760 (-129ø41'48.34")
NOM_PIXEL_SPACING = 6.2500000
NOM_LINE_SPACING = 6.2500000
PRODUCT_REFERENCE = PATH IMAGE (SGF)
INSTRUMENT = SAR FINE 4 BEAM
ORBIT_NUMBER = 4424

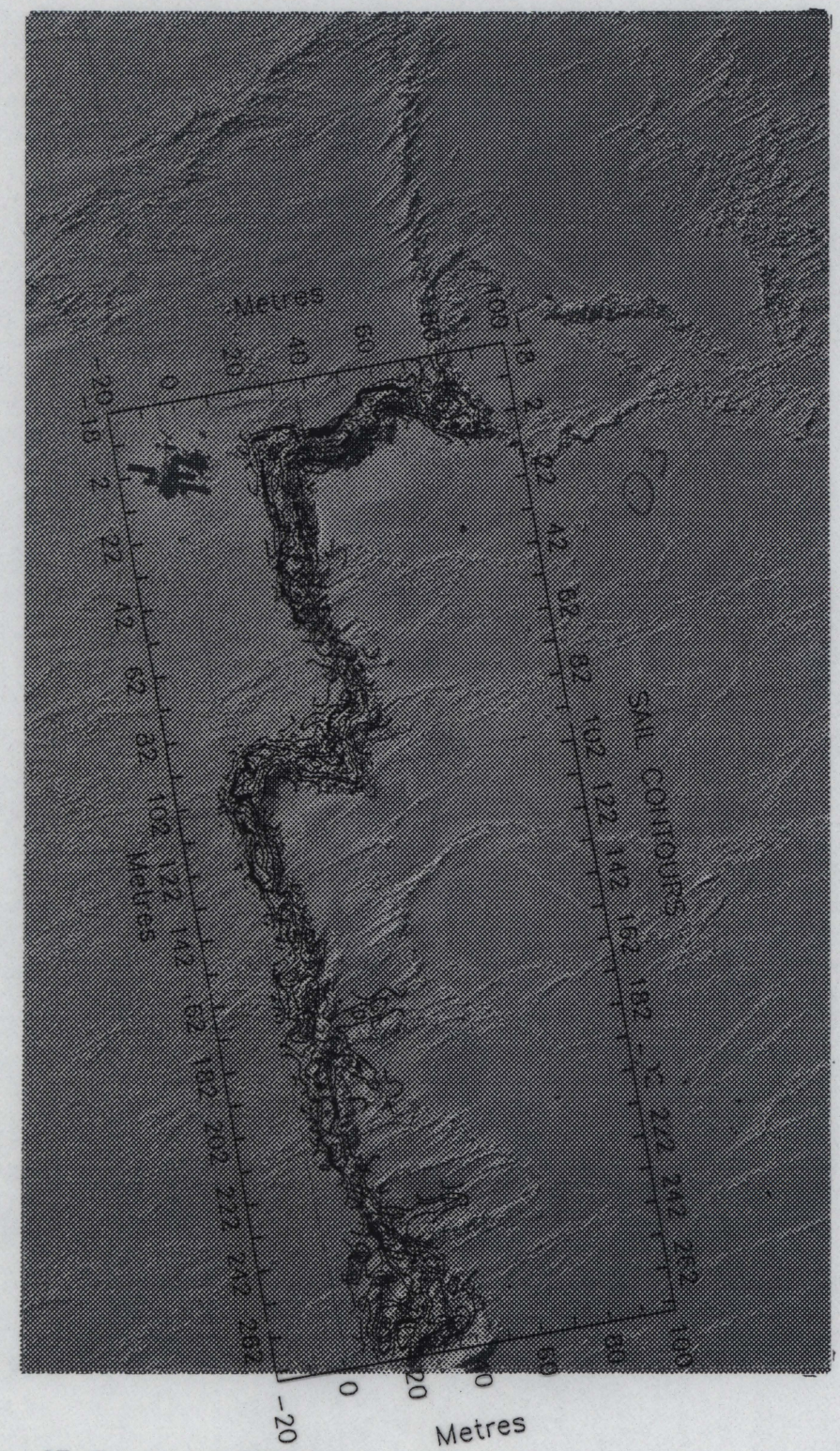

Figure 37: Overlay of DTM Contour Map onto Air Photograph of Study Site.

ORBIT_DIRECTION = ASCENDING
DATE_AQUIRED = SEPTEMBER 09 1996
DATE_PROCESSED = OCTOBER 08 1996

APPENDIX I Continued

RADARSAT Scene Specifications

Descending Imagery

FILE_TYPE = IMAGE
IMAGE_POINTER = SCENE01\DAT_01.001
SCENE_ID = C0003343
LABEL_RECORDS = 1
LABEL_RECORD_BYTES = 16252
LINE_PREFIX_BYTES = 192
GROUP _SAMPLES = 1
BAND_TYPE = BSQ
IMAGE_BANDS = 1
SAMPLE_BITS = 16
SAMPLE_BITS_USED = 16
SAMPLE_TYPE = UNSIGNED_INTEGER
BYTE_ORDER = MSB
SEMI_MAJOR_AXIS = 6378.140
SEMI_MINOR_AXIS = 6356.755
PLATFORM = RADARSAT_1
IMAGE_RECORD_BYTES = 16110
IMAGE_LINES = 8402
LINE_SAMPLES = 7959
SCENE_ORIENTATION = 8.6517572
SCENE_CENTRE_LAT = 57.717010 (57ø43'01.23")
SCENE_CENTER_LON = -129.670494 (-129ø40'13.78")
UL_CORNER_LAT = 57.983072 (57ø58'59.06")
UL_CORNER_LON = -130.018739 (-130ø01'07.43")
UR_CORNER_LAT = 57.915800 (57ø54'56.88")
UR_CORNER_LON = -129.188382 (-129ø11'18.18")
LL_CORNER_LAT = 57.517003 (57ø31'01.21")
LL_CORNER_LON = -130.147721 (-130ø08'51.80")
LR_CORNER_LAT = 57.449800 (57ø26'59.28")
LR_CORNER_LON = -129.328080 (-129ø19'.41.09")
NOM_PIXEL_SPACING = 6.2500000
NOM_LINE_SPACING = 6.2500000
PRODUCT_REFERENCE = PATH IMAGE (SGF)
INSTRUMENT = SAR FINE 4 BEAM
ORBIT_NUMBER = 4474

ORBIT_DIRECTION = DESCENDING
DATE_AQUIRED = SEPTEMBER 12 1996
DATE_PROCESSED = OCTOBER 08 1996

Appendix II
Image Statistics

	*Ascending Image**	*Descending Image**	*First Principal Component Image*	*Final Fused Image*
Number of Pixels	6500000	6500000	6500000	6500000
Minimum Pixel Value	5	0	1189	1189
Maximum Pixel Value	65535	43167	44416	47688
Mean Pixel Value	11233.51	9397.39	32755.16	33910.09
Median Pixel Value	11225	10545	31283	32984
Standard Deviation	4906.56	5815.74	5862.45	6052.48

***After speckle removal**

Appendix III
Computer Processing Parameters

PCI Routine

TEX Texture Analysis — Radar Analysis Package

Parameters

Textural Measure	12	Grey Level Difference Vector (GLDV), Contrast
Filter Size	7X7	
Spatial Relationship	default (1)	

PCI Routine

LINE Lineament Extraction — Image Processing Package

Parameters

Radius of Filter	20
Threshold of Edge Gradient	120
Threshold for Curve Length	10
Threshold for Line Fitting Error	3
Threshold for Angular Difference	30
Threshold for Linking Distance	30

PCI Routine

PCA Principal Component Analysis — Multispectral Analysis Package

Parameters

Midpoint	default (32767.5)
Range of Standard Deviations Retained	no entry (all)

Appendix IV.

PCA Principal Component Analysis V6.3 EASI/PACE 15:37 08Jan2001

/work_rsykes/corrected_ascending_descend[S 11BIC 2600P 2500L] 28Sep1999

Input Channels: 1 2
Output Channels: 10 11
Eigenchannels : 1 2

Sampling Window: 0 0 2600 2500
Sample size : 813800

Channel	Mean	Deviation
1	0.1123377E+05	0.4908274E+04
2	0.9385194E+04	0.5822802E+04

Covariance matrix for input channels:

	1	2
1	0.240912E+08	
2	0.236332E+07	0.339050E+08

Eigenchannel	Eigenvalue	Deviation	%Variance
1	0.3444449E+08	0.5868943E+04	59.39%
2	0.2355168E+08	0.4853008E+04	40.61%

Eigenvectors of covariance matrix (arranged by rows):

-0.22254 -0.97492
-0.97492 0.22254

Scaling Information:

Eigen Channl	Output Channl	--------Unscaled-------- Min	Max	Deviation Range	Midpoint Factor	Scale
1	10	-0.3157831E+05	0.1164872E+05	all	32767.500	1.000
2	11	-0.5502813E+05	0.1547656E+05	all	32767.500	1.000

Appendix V.
Raw Texture Classification Statistics

Texture Classified Unfiltered Ascending RADARSAT imagery (Case 1)

#Pixels Classified as Forest	55646
#Pixels Classified as Non-Forest	11330

Texture Classified Unfilterd Descending RADARSAT imagery (Case 2)

#Pixels Classified as Forest	54925
#Pixels Classified as Non-Forest	12051

Texture Classified Despeckled Ascending RADARSAT imagery (Case 3)

#Pixels Classified as Forest	1883
#Pixels Classified as Non-Forest	65093

Texture Classified Fused RADARSAT imagery (Case 4)

#Pixels Classified as Forest	33110
#Pixels Classified as Non-Forest	33866

Classified Thematic Mapper Imagery		Less Texture Classified Forest			
		Case 1	Case2	Case 3	Case 4
#Pixels Classified as Forest	48786	3402	3697	47930	21575
#Pixels Classified as Water	2888	2763	2792	2859	2718
#Pixels Classified as Barren	11542	3828	3743	10862	7492
#Pixels Classified as Rock/Beach	3760	1337	1819	3442	2081

VITA

Surname: Sykes Given Names: Richard John

Place of Birth: Victoria, British Columbia, Canada

Educational Institutions Attended:

University of Victoria	1975 to 1980
University of Victoria	1995 to 2001

Degrees Awarded:

B.Sc.	University of Victoria	1980

PARTIAL COPYRIGHT LICENSE

I hereby grant the right to lend my thesis to users of the University of Victoria Library, and to make single copies only for such users or in response to a request from the Library of any other university, or similar institution, on its behalf or for one of its users. I further agree that permission for extensive copying of this thesis for scholarly purposes may be granted by me or a member of the University designated by me. It is understood that copying or publication of this thesis for financial gain shall not be allowed without my written permission.

Title of Thesis:

Improving the Classification of High Relief RADARSAT Imagery Through the Fusion of Ascending and Descending Look Angle Images

Author 

Richard John Sykes

July 31, 2001